THE ASTROPHYSICAL JOURNAL, 429:672–693, 1994 July 10

ATOMIC AND MOLECULAR GAS IN INTERSTELLAR CIRRUS CLOUDS

WILLIAM T. REACH,[1] BON-CHUL KOO,[2] AND CARL HEILES[3]
Received 1993 May 24; accepted 1994 January 18

ABSTRACT

The dust, atomic gas, and molecular gas content of a sample of 26 of isolated, degree-sized infrared clouds are compared. Half of the clouds have an infrared excess indicating the presence of H_2, and 14 contain compact CO-emitting regions. Complete, high angular resolution H I and CO maps of one cloud, G236+39, resolve the transition between atomic and molecular H, as well as the location of CO formation. Assuming the infrared emission traces the total column density, H_2 is inferred to be much more widely distributed than the CO. The CO rotational levels are subthermally excited, and the (2–1)/(1–0) line ratios suggest a density $n(H_2) \sim 200$ cm^{-3} where CO was detected. A model of H_2 formation on grain surfaces balanced by self-shielded photodissociation fits the variation of infrared brightness with H I column density. Assuming a temperature of 80 K, typical of diffuse H_2 (Savage et al. 1977), the H_2 chemistry requires an average density $n(H + 2H_2) \sim 50$ cm^{-3}. For G236+39, if the distance is 100 pc, the H I and H_2 masses are estimated to be 90 and 70 $M_\odot$, respectively. High-resolution H I and infrared maps of a smaller cloud, G249.0+73.7, reveal no evidence for molecular gas, which is likely due to the low total column density through this cloud. These results suggest the H_2 and H I content are comparable for some interstellar cirrus clouds with column densities $N(H\ I) > 4 \times 10^{20}$ cm^{-2}, even where CO was not detected.

Subject headings: dust, extinction — ISM: clouds — ISM: molecules — radio lines: ISM

1. INTRODUCTION

The hydrogen in an interstellar cloud exposed to the interstellar radiation field is primarily atomic down to a certain depth, where the extinction (by dust and self-shielding) of the radiation field is large enough that the H_2 formation rate exceeds its photodissociation rate. Molecules other than H_2 form deeper into a cloud, and some molecules, such as CO, are capable of self-shielding when its lines become opaque to those photons in the narrow energy ranges capable of dissociating them. The purpose of the project described in this paper was to determine the locations, within nearby interstellar clouds, where the gas changes from predominantly atomic to molecular form. The distribution of the most abundant molecule, H_2, cannot be mapped for cold ($< 10^3$ K) clouds because the H_2 molecule is symmetric, eliminating dipole transitions between low-lying rotational energy levels. We observed the transition from atomic to molecular H indirectly, by comparing the distribution of 21 cm line emission—which traces the column density of atomic gas—and infrared surface brightness—which traces the total column density interstellar dust (and its associated gas).

Previous studies (cf. Spitzer & Jenkins 1975; Savage et al. 1977; Federman, Glasgold, & Kwan 1979) of the transition from atomic to molecular gas have been based on ultraviolet absorption-line observations of H I (Lyman-α) and H_2 ([1,0] Lyman band) for stars with a range of total column density. These studies have the advantage that the H_2 (and other molecules) as well as the H I are observed directly, often in their ground states, within the same, pencil beam. Comparison of lines of sight toward over 100 stars revealed that the fraction of H in molecular form, $2N(H_2)/[2N(H_2) + N(H\ I)]$, increases from less than 1% to greater than 1% when $2N(H_2) + N(H\ I) \gtrsim 5 \times 10^{20}$ cm^{-2} (Savage et al. 1977). The kinetic temperature of the clouds containing the H_2 can also be determined from ultraviolet spectra, because transitions from both the $J = 0$ and $J = 1$ rotational levels are accessible. The mean kinetic temperature was found to be 77 ± 17 K for diffuse clouds (Savage et al. 1977).

A disadvantage of the optical studies is that they rely on the comparisons among lines of sight to stars behind a range of clouds. Each line of sight requires an early-type star (with sufficient ultraviolet flux to allow narrow absorption lines to be detected), and these stars locally enhance the radiation field. Comprehensive models of the chemistry toward the best-studied stars (van Dishoeck & Black 1986) assume radiation fields enhanced by a factor of 2 (for ζ Oph) to 8 (for χ Oph). Further, the optically selected lines of sight are essentially randomly placed with respect to the interstellar clouds they are probing. It is not possible to understand cloud structure, or the transition from atomic to molecular gas in clouds, using only single lines of sight through clouds. The fraction of the sky covered by the CO-emitting regions of the clouds discussed in this paper is so small that it would be impossible to study them using absorption lines alone—there are not enough early-type stars. Emission-line surveys of individual clouds allow the various chemical species to be mapped and compared within individual clouds.

We had previously identified a sample of isolated interstellar clouds for detailed study (Heiles, Reach, & Koo 1988, hereafter HRK). The selection criteria were that each cloud be an isolated, centrally condensed, approximately degree-sized feature in the 100 μm all-sky survey by the *Infrared Astronomical Satellite* (*IRAS*) (Neugebauer et al. 1984). Furthermore, the clouds were required to be isolated from extensive H I structures evident on the 21 cm Hat Creek all-sky survey (Heiles & Habing 1974). By comparing their 21 cm lines and 100 μm brightnesses, we found that several clouds have large infrared

[1] NASA/Goddard Space Flight Center, Code 685 Greenbelt, MD 20771; also Astronomy Department, University of California-Berkeley.
[2] Seoul National University, Astronomy Department, Seoul 151-742, Korea; also Astronomy Department, University of California-Berkeley and Harvard-Smithsonian Center for Astrophysics.
[3] Astronomy Department, University of California Berkeley, CA 94720.

emission relative to their H I column density. If the infrared emission per H atom is the same for all clouds, and the infrared excess is due to dust associated with molecular gas, then the molecular fraction of the clouds ranges from zero to ~50%.

Other observational studies of infrared-selected clouds, with some overlap with the HRK sample, have suggested that infrared excess is a tracer of molecular gas. When an infrared map of the Ursa Major region was compared to CO and H I maps with similar angular resolutions, it was found that while neither gas map cloud match the features in the infrared map, a linear combination of the CO and H I maps could (de Vries, Heithausen, & Thaddeus 1987). This approach was applied to the entire sky to make a complete survey of molecular gas at high latitudes, by subtracting the atomic gas–correlated infrared emission (traced by the H I 21 cm line) from the *IRAS* 100 μm all-sky map (Désert, Bazell, & Boulanger 1988). In a subsequent radio CO survey of the infrared excess clouds, only 13% were detected (Blitz, Bazell, & Désert 1990), suggesting that either (1) the infrared excess is tracing something other than molecular gas or (2) the CO does not trace all of the molecular gas. The results of an extensive, low-resolution CO survey of molecular gas at high latitudes (Heithausen et al. 1993) have cast doubt on whether the faintest infrared excess clouds are real, because the infrared excess was found to be a poor guide to the CO emission. (This can be explained partially by the fact that the CO survey of Heithausen et al. is sensitive to smaller H_2 column densities than the infrared excess clouds listed by Désert et al., and partially by the fact that the faintest infrared excess clouds may be spurious—due to scan-to-scan calibration errors in the *IRAS* and H I data.) In this work, we directly address the question of whether CO traces molecular gas, using high angular resolution H I 21 cm line observations and multitransition CO line observations of one of our clouds.

2. OBSERVATIONS

2.1. CO *Survey of Selected Cirrus Clouds*

In order to determine the molecular content and morphology of cirrus clouds, molecular line maps of each cloud with angular resolution comparable to *IRAS* (~3′) are desired. This is not yet practical for the cirrus clouds because of their large angular size. The amount of time required to map a square degree of sky with sufficient sensitivity (0.1 K rms brightness temperature) and spectral resolution (<0.5 km s^{-1}) varies from 50 days to 2 hr, depending on the receiver sensitivity, weather, and telescope diameter. The fastest mapping rate is for small telescopes with sensitive receivers. However, if the CO-emitting regions of cirrus clouds are smaller than the beam, then the maps with small telescopes will be inadequate.

We observed all of our clouds for CO(1–0) emission using the NRAO 12 m (beamwidth 1′) and CfA 1.2 m (beamwidth 9′) telescopes. At NRAO, we observed the 100 μm surface brightness peaks of each cloud, first using a wide bandwidth (167 km s^{-1} total) to locate the lines (1987 July), then following up with higher resolution (0.26 km s^{-1} per channel) to resolve the lines (1988 June). Integrations were performed only until adequate signal-to-noise ratio was achieved; for nondetections, the rms fluctuations in the spectra were 0.15 K or better. For most clouds, we also observed one-dimensional cuts through the infrared peaks, and for some clouds we made small rectangular grids. Positions with the brightest CO lines for each cloud were also observed for ^{13}CO. These integrations were continued until the line was detected; for nondetections, the rms fluctuations were less than 0.05 K. CfA 1.2 m observations (1990 December) were a combination of single pointings and rectangular (9′ spacing) grids.

Finder charts for our CO observations with the NRAO 12 m are shown in Figure 1. These figures were made at the same angular scale for direct comparison. The gray scale and contours are 100 μm surface brightness from the *IRAS* Sky Survey Atlas (Wheelock et al. 1991, hereafter ISSA). Circles mark the CO-observed positions, and filled circles indicate detections. The irregular combination of pointed observations, 4′ spacing scans, and 1′–4′ grids is a reflection of our "hunt-and-peck" observing strategy. It is possible that some CO emission was missed, especially in clouds with only a few pointed observations.

The results of the survey are summarized in Table 1. For detected clouds, a Gaussian fit to a representative CO profile and the angular extent over which CO was detected is given. For all clouds, the number of points that were observed with each telescope is given. Note that nondetections with only a few points are inconclusive, because we may have missed the CO-emitting region. Nondetections that were confirmed with the CfA 1.2 m telescope (whose large beam could not miss the CO) are more conclusive, but these observations suffer from beam dilution because the CO-emitting regions are typically smaller than the beam.

Some of these clouds have been observed by others. G225.6−66.4 was mapped at 9′ resolution (Keto & Myers 1986); the CO-emitting region is two unresolved clumps in their map (despite the fact that it is listed as 17′ radius in their table). This cloud was also observed at 44″ resolution (Stark 1993), revealing a size of 6′ for one of the bright cores. G228.0−28.6 and G230.1−28.4 were mapped at 44″ resolution (Stark 1993), revealing emitting regions about 5′ in size (FWHM) for each. G90.0+38.8 and G94.8+37.6 are part of the Draco nebula, which has extensive CO emission (Rohlfs et al. 1989; Herbstmeier, Heithausen, & Mebold 1993).

2.2. *Complete* CO *and* H I *Maps of* G236+39

In order to investigate the detailed relationship between atomic and molecular gas and dust emission, we desire sensitive observations of all three components at the best common resolution. In order to obtain sufficient resolution in the 21 cm line, it is necessary to use the largest telescope available. Interferometry is difficult because it lacks sensitivity and field of view. (One cloud, G86.5+59.6, was observed with the DRAO Synthesis Telescope [Martin et al. 1993]; this cloud is apparently purely atomic, based on its "normal" infrared emission per unit H I column density [HRK] and lack of CO emission [Table 1], so we will not discuss this cloud further here.) The largest (single-dish) telescope available for H I observations is the NAIC Arecibo 305 m, telescope, with its 3′ resolution. Only clouds in the declination range 0°–40° can be observed with this telescope, and we mapped both such clouds in our sample. One of these, G249.0+73.7, is a very low column density cloud that is apparently totally atomic. We obtained 132 H I spectra for this cloud in 1987 November, and they are compared to the infrared data below. The other cloud accessible at Arecibo, G236+39, contains CO and has infrared excess. An infrared map of the cloud is shown in Figure 2.

2.2.1. *Arecibo 21 Centimeter Emission Observations*

G236+39 was completely mapped in 1990 October using drift scans sampled every 6 s in time (1.′5), for a total of over 9000 spectra, using the dual circular polarization feed. Drift

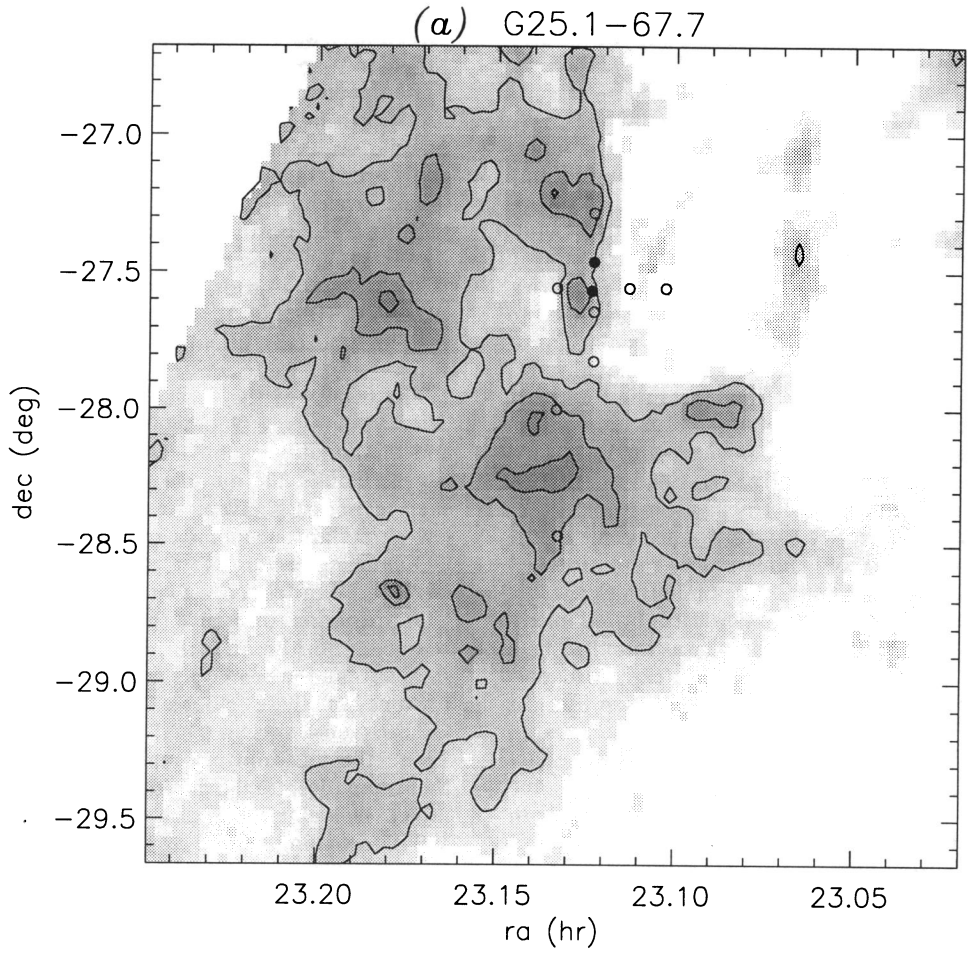

FIG. 1*a*

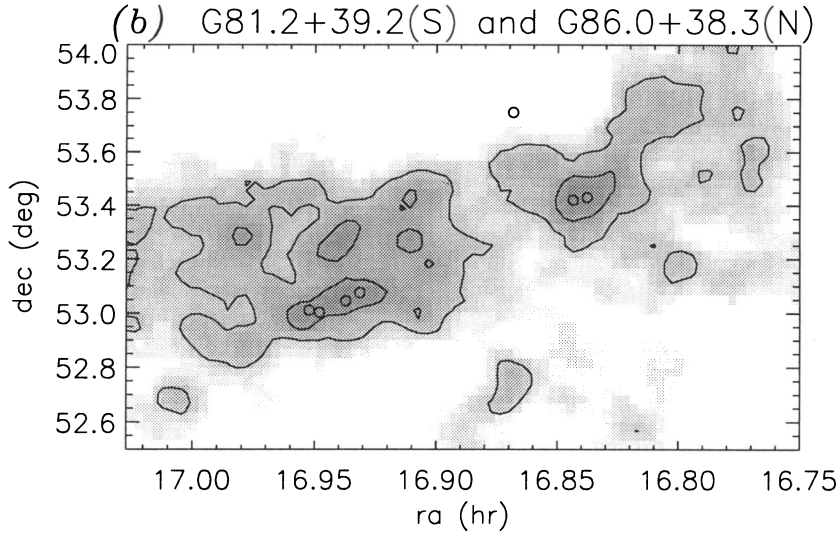

FIG. 1*b*

FIG. 1.—Maps of the 100 μm surface brightness of isolated cirrus clouds. The gray scales are linear, with a dynamic range of 0–10 MJy sr^{-1}, and the contours are spaced by 0.5 MJy sr^{-1}, except for panels Figs. 1*f* and 1*m*, which have contours every 1 MJy s^{-1}. All maps are at the same scale (arcmin mm^{-1}) for comparison. The locations of the NRAO CO(1–0) observations are indicated by circles, with filled circles indicating detections.

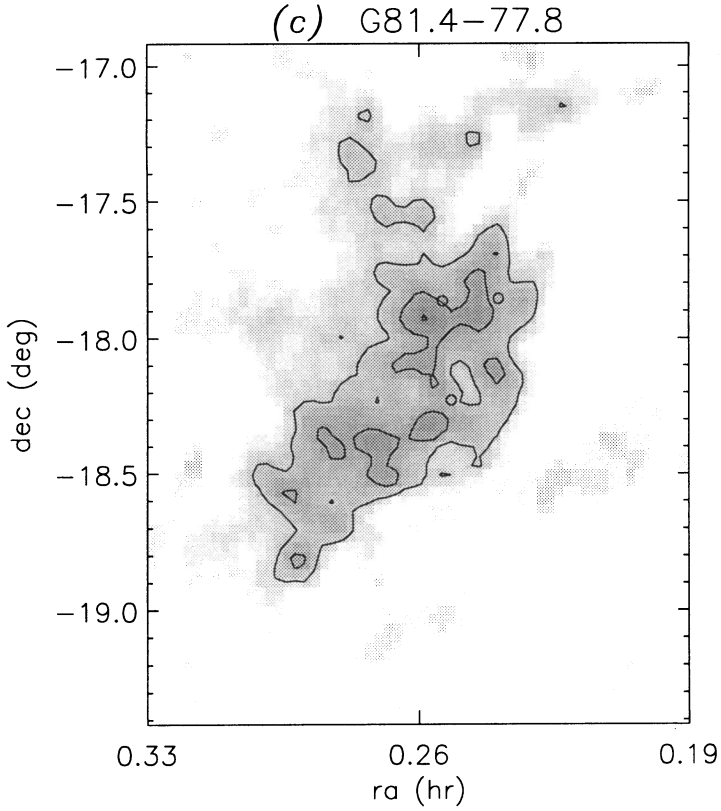

FIG. 1c

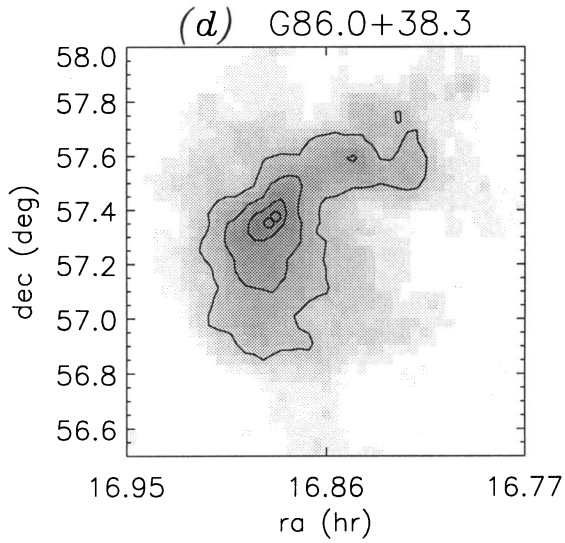

FIG. 1d

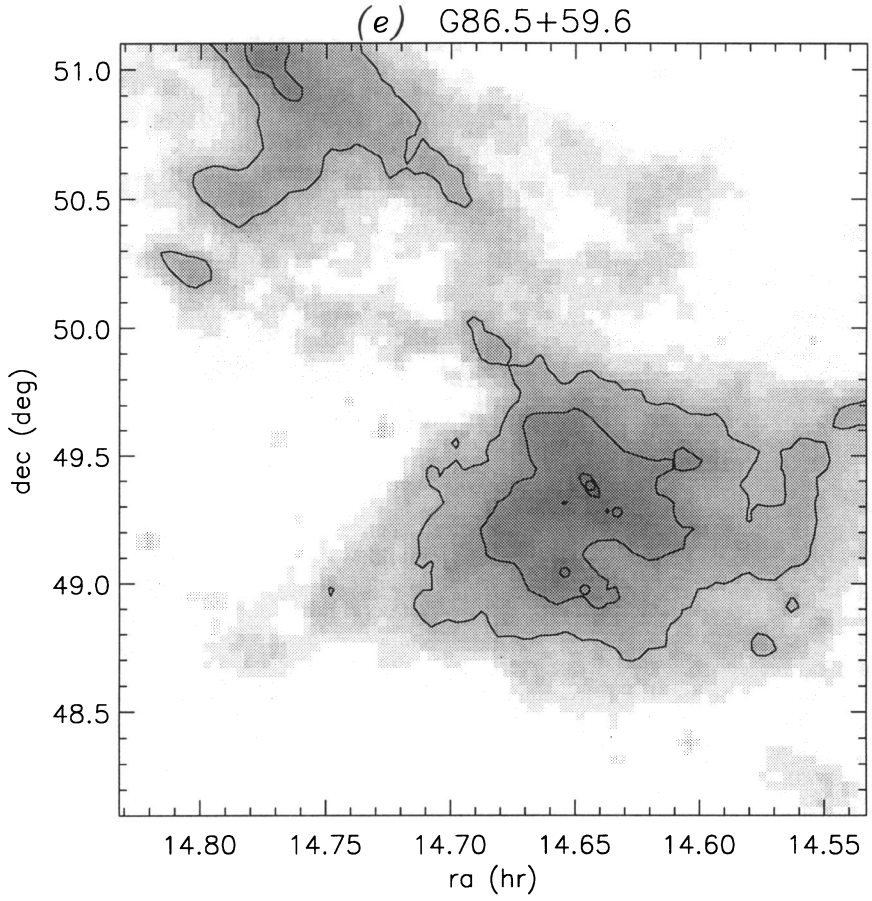

FIG. 1e

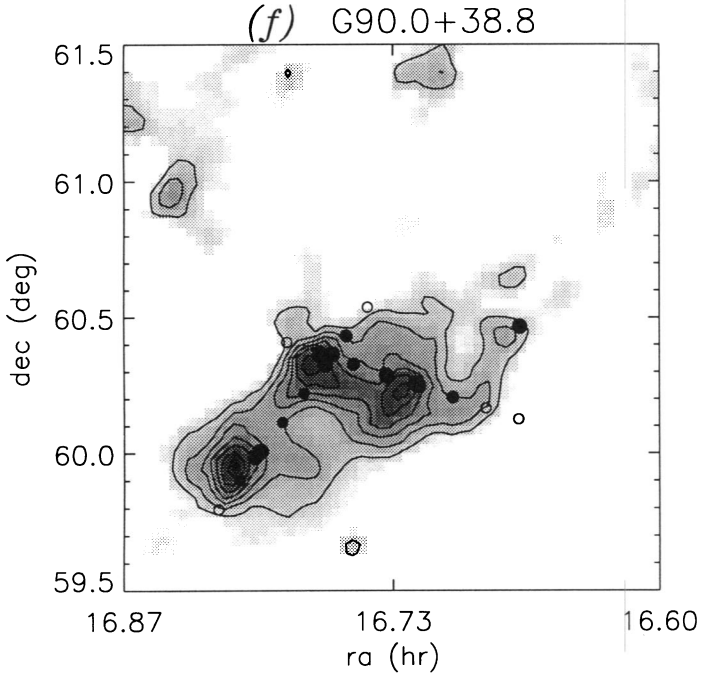

FIG. 1f

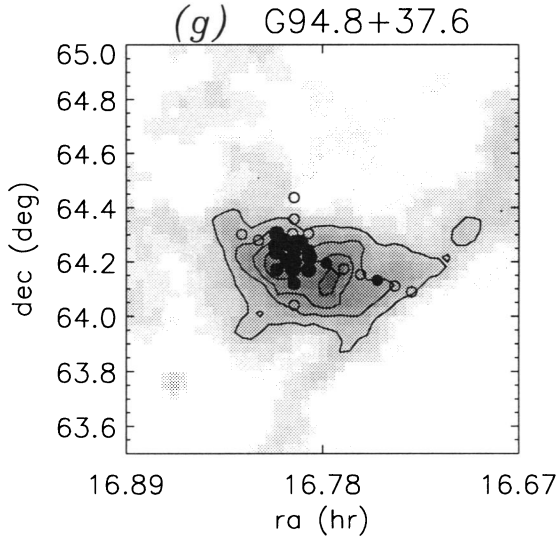

FIG. 1g

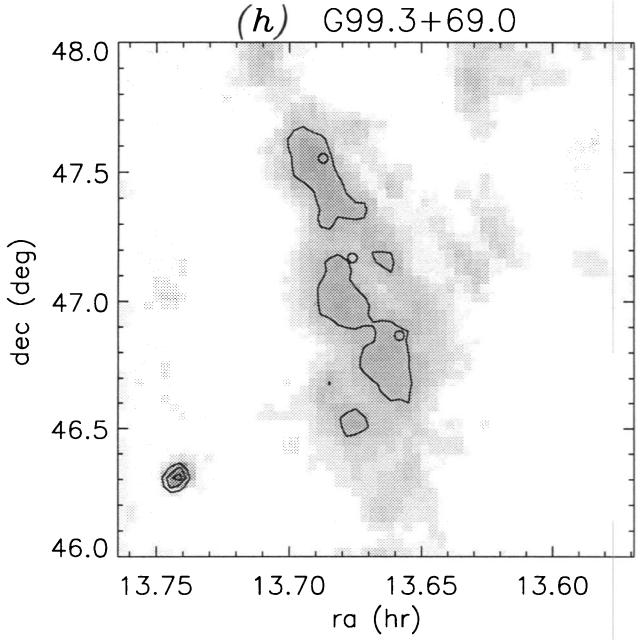

FIG. 1h

scans were obtained as total power spectra, and these were calibrated relative to a noise diode using OFF-frequency spectra taken just before and after each scan. The cloud may be divided into three main components: the southern cloud (which contains the CO emission), the northern cloud (which contains the brightest H I emission), and a faint eastern cloud. The northern and southern clouds were listed separately in HRK, with names G235.0+38.7 and G235.9+38.2, respectively. Sample 21 cm spectra toward the three cloud components, as well as a position outside the cloud, are shown in Figure 3. Apart from a very broad spectral line (FWHM 13 km s^{-1}), which may be attributed to warm, diffuse H I along the line of sight, all of the 21 cm line emission is due to G236+39.

The beam efficiency and stray radiation contribution were estimated by comparing our spectra to those in the Bell Labs all-sky survey (Stark et al. 1992). After convolving our spectra with a crude approximation of the Bell Labs beam (2°.2 Gaussian), we found a relative beam efficiency for our data of 0.8; this agrees with previous estimates for the 21 cm dual circular feed (cf. Dickey 1977). The brightness temperature is related to our observed antenna temperature by $T_B \approx T_A/0.8$. The Arecibo and Bell Labs profiles are similar, and there is no evidence for "stray" radiation (such as Galactic plane H I lines scattered off the platform and towers into the beam). In fact, the Bell Labs profiles are more extended than our Arecibo profiles, suggesting that our baselines subtracted some real emission at $V < -20$ and $V > 15$ km s^{-1}. The column density in these wings is small ($< 10^{19}$ cm^{-2}), so they have no impact on the work described in this paper.

2.2.2. *Arecibo 21 Centimeter Absorption Measurements*

There are several continuum sources within the region mapped at Arecibo. These objects are almost certainly extragalactic, and their emission is absorbed by the H I along the line of sight. None of the sources are much brighter than the 21 cm line emission itself. The brightest, 3C 230, has a flux of 3 Jy and an observed antenna temperature of about 10 K at a zenith angle of 19° (near the edge of the dish). We observed the four brightest continuum sources behind G236+39, together with hexagonal patterns of reference positions surrounding each source, using in-band frequency switching. We also observed 3C 237, a source with known strong absorption (Dickey 1977), to test our observing procedures and methods. The Hanning-smoothed, single-channel rms brightness fluctuations in the emission spectra are ~0.3 K, about 3% of the average 21 cm line brightness. No absorption features are

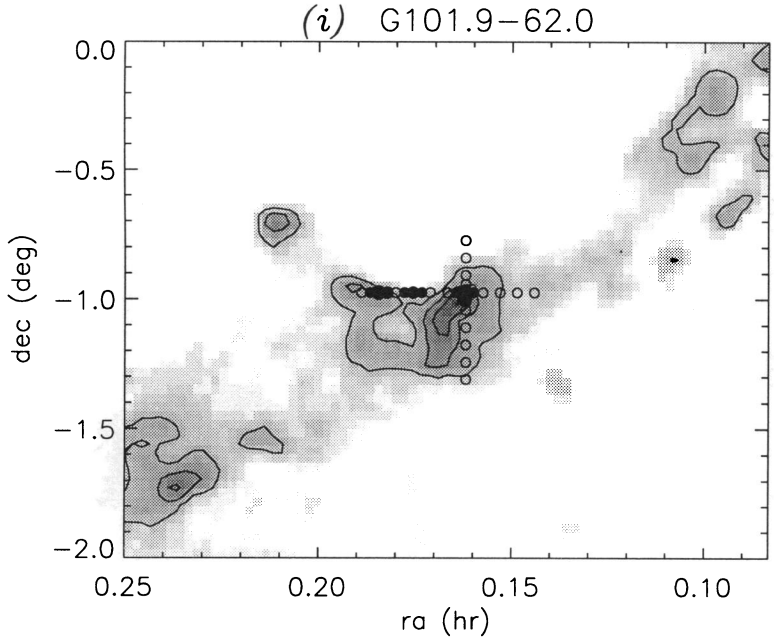

FIG. 1*i*

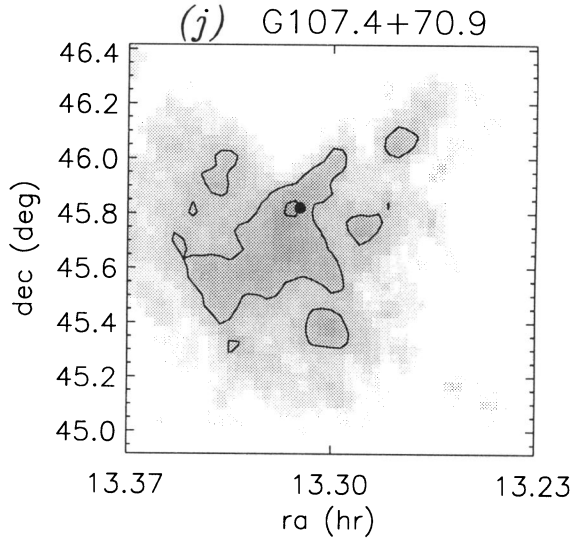

FIG. 1*j*

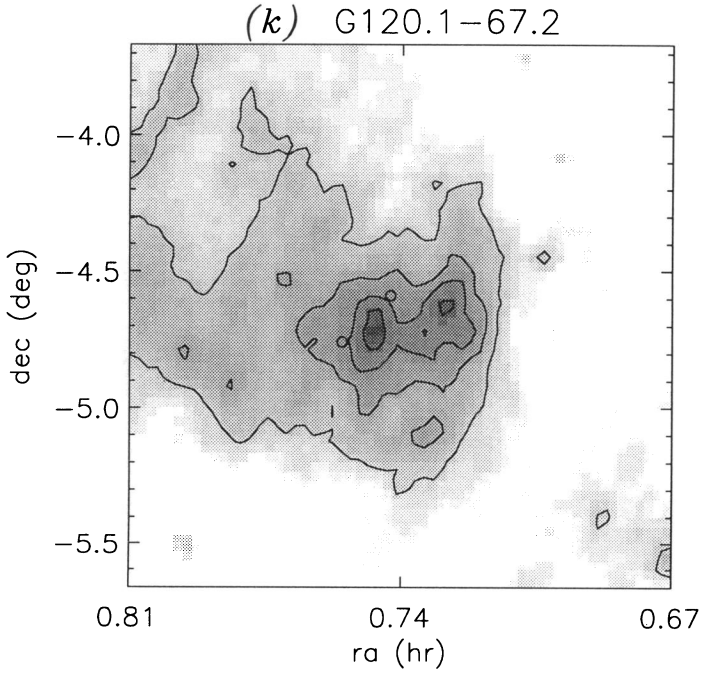

FIG. 1*k*

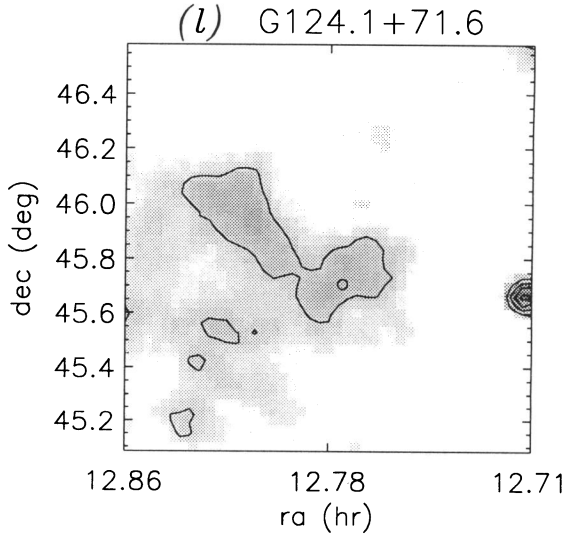

FIG. 1*l*

present in the spectra of the continuum sources behind G236+39; the results are described more fully in § 3.2. The deep absorption line in 3C 237 has an apparent optical depth of 0.3, in agreement with previous results (cf. Dickey 1977), suggesting the observing procedure was not flawed.

2.2.3. *Kitt Peak* CO *Observations*

The CO(1–0) 115.2712 GHz emission from G236+39 was mapped using the NRAO 12 m telescope in 1990 May. All far-infrared *IRAS* point sources and extended 100 μm surface brightness peaks were observed. Also two long scans, one through the southern cloud and one through the northern cloud, were made at 4′ spacing. Finally, the southern cloud was mapped at 2′ spacing throughout and 1′ spacing in selected regions. The rms fluctuations in the spectra were typically 0.15 K. The CO(1–0) line integral map of the southern portion of G236+39 is shown in Figure 4*a*. All of the CO(1–0) peaks were also observed in the ^{13}CO(1–0) line, and a strip of ^{13}CO(1–0) observations was performed through the entire CO-emitting region along declination 00°45′; the rms fluctuations in the ^{13}CO(1–0) spectra were typically 0.07 K.

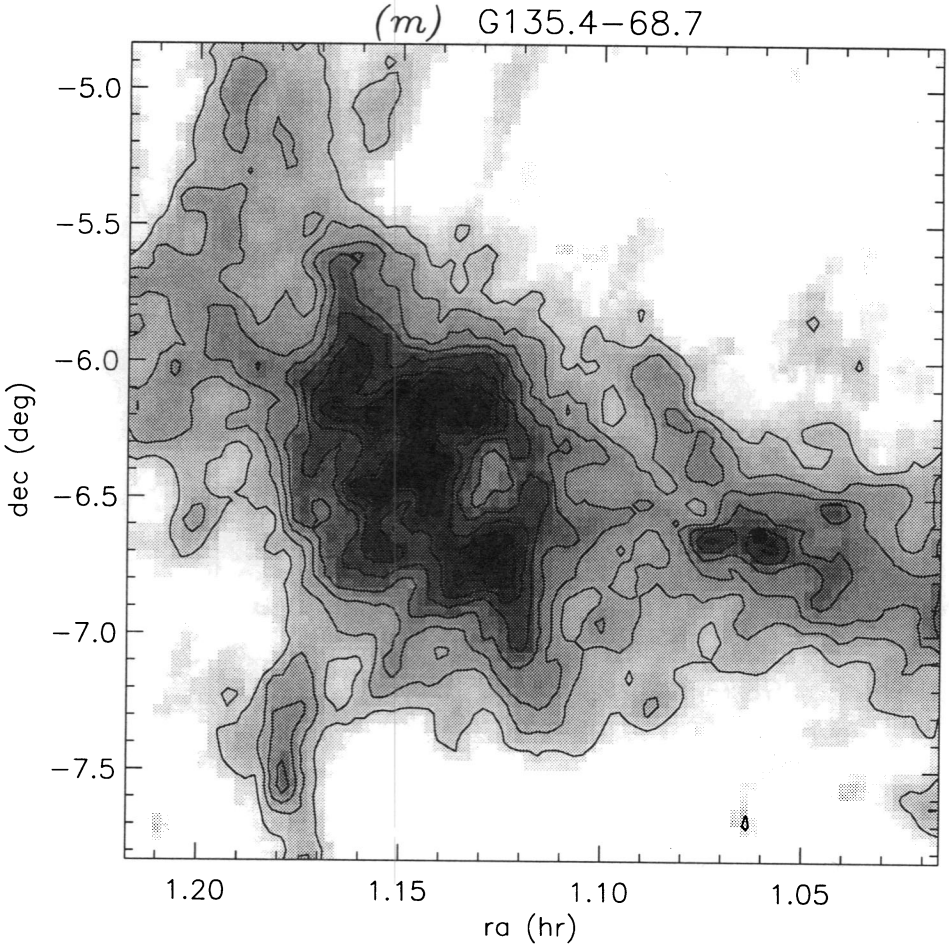

FIG. 1*m*

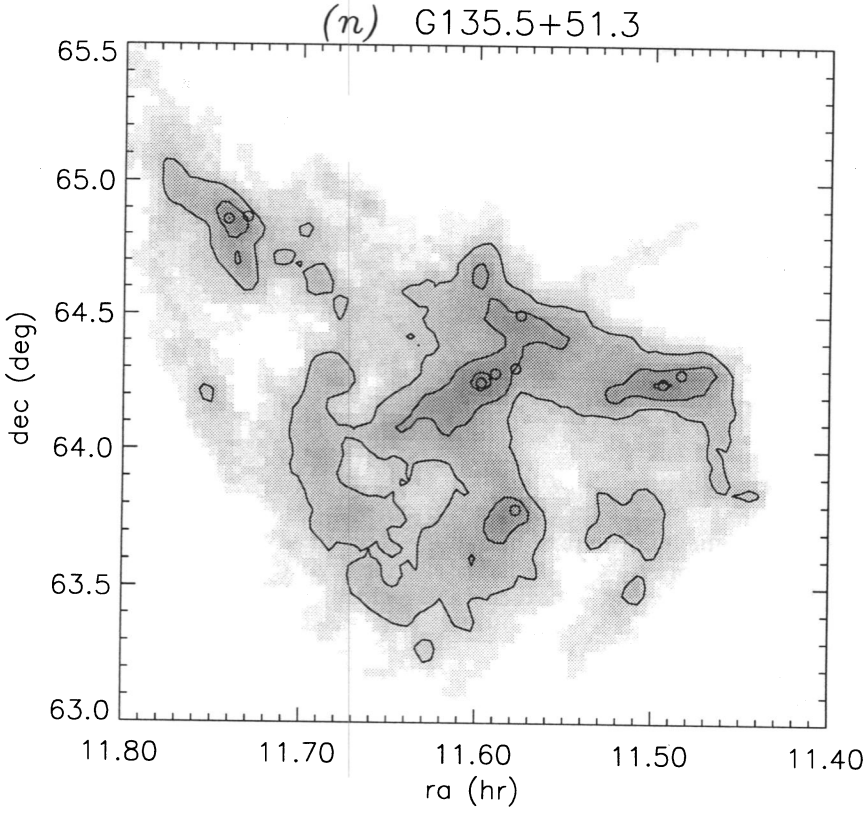

FIG. 1*n*

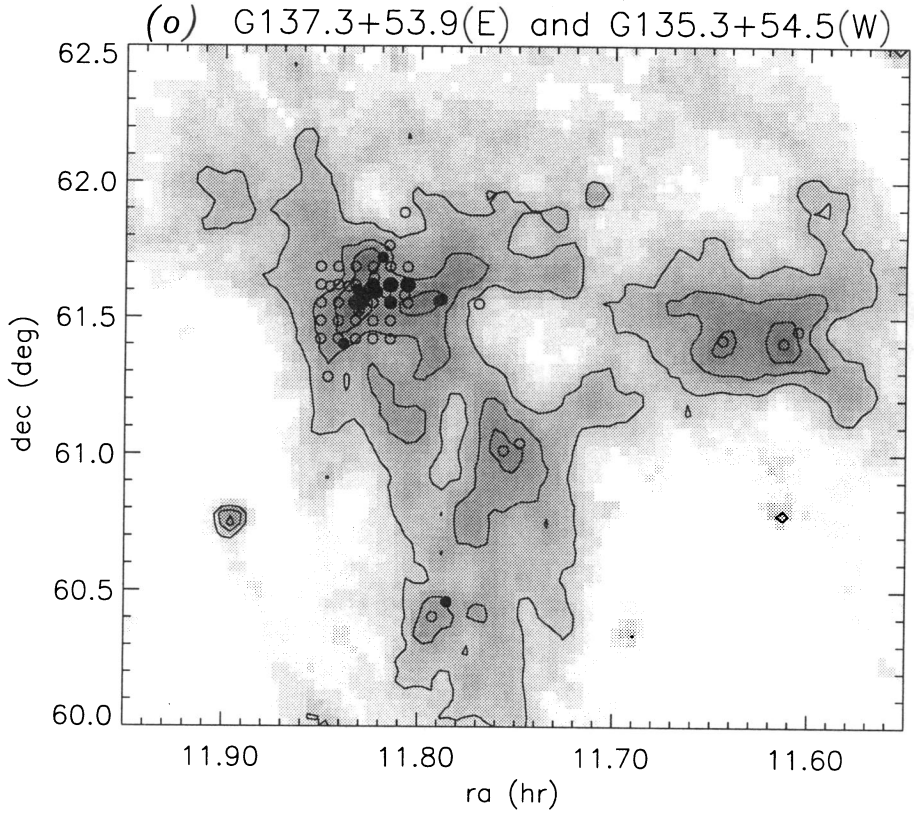

FIG. 1*o*

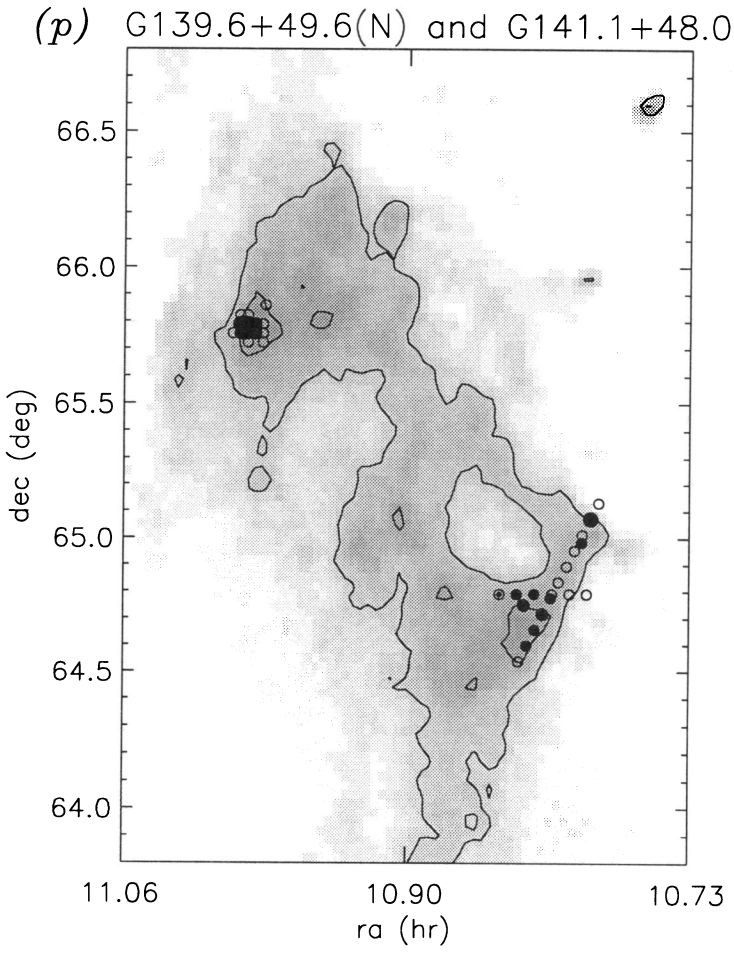

FIG. 1*p*

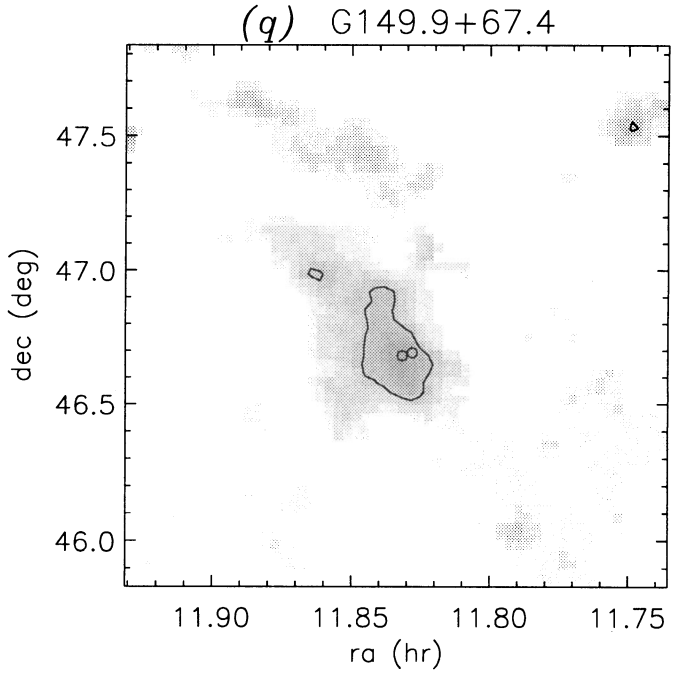

FIG. 1*q*

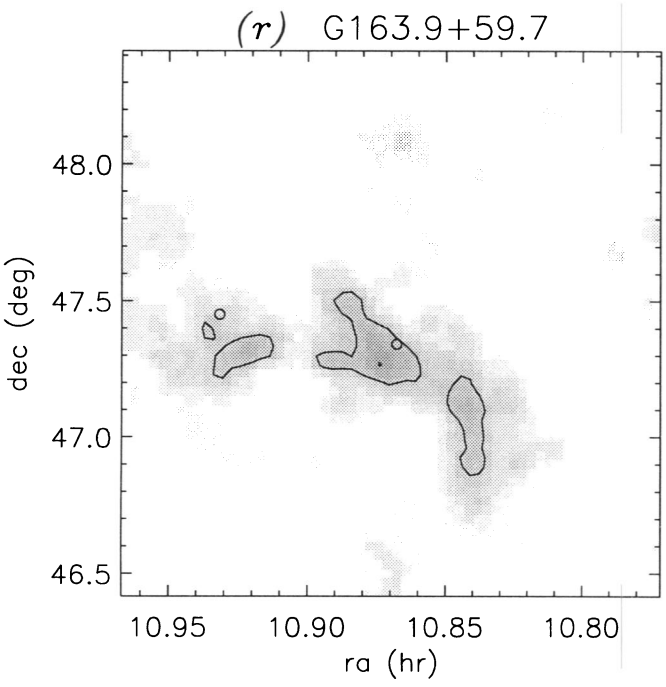

FIG. 1r

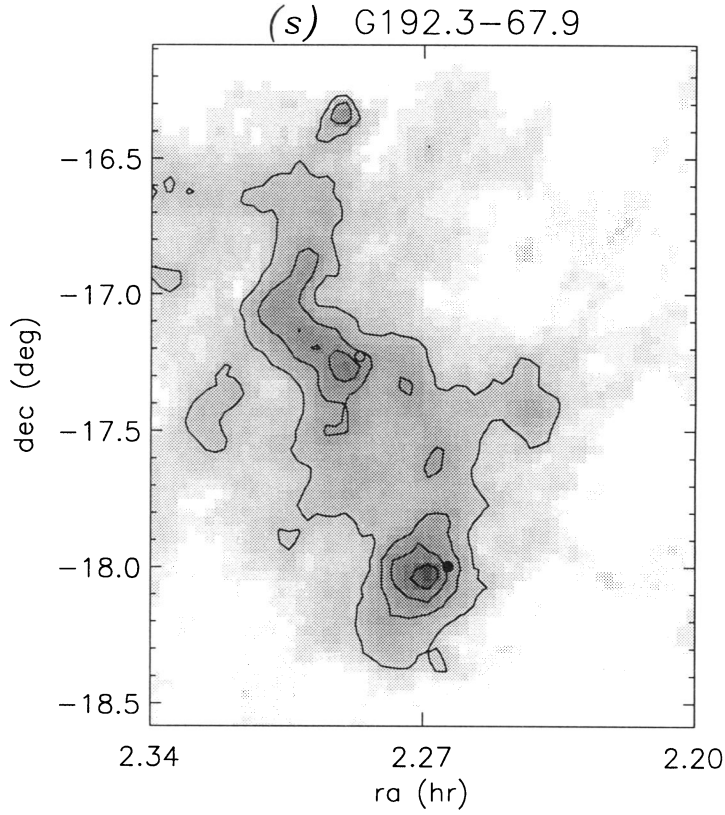

FIG. 1s

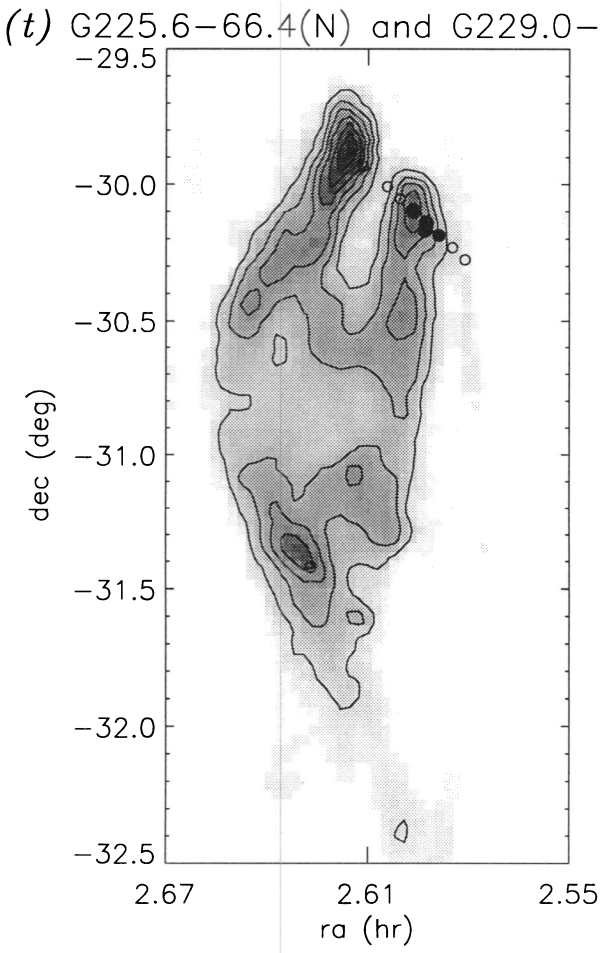

FIG. 1t

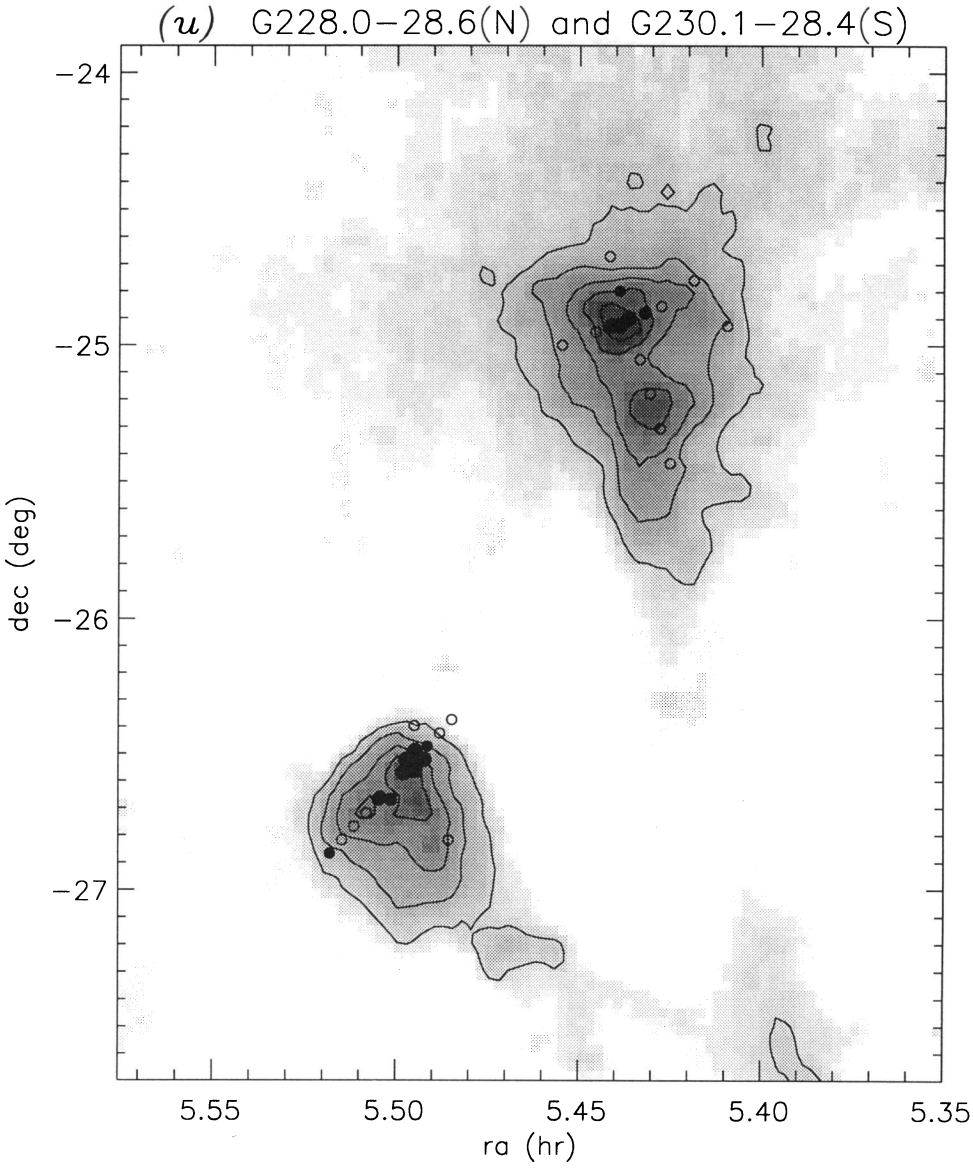

FIG. 1*u*

Additional observations of the CO(2–1) and ^{13}CO(2–1) lines were made toward the peaks of the CO(1–0) emission and the center of the southern cloud (1993 February). The CO line spectra of some positions in the cloud are shown in Figure 5. The line shape, centroid, and width vary substantially from clump to clump. The profile for clump B has almost no overlap with that for clump N, although they are $\lesssim 30'$ apart. The ^{13}CO lines are somewhat narrower than their CO counterparts, as is expected if the CO lines are optically thick. The most narrow line by far is the ^{13}CO(2–1) line, at only 0.3 km s^{-1}. The peak brightness, linewidth (FWHM), and line integral for the positions of brightest CO(1–0) and the position of largest infrared excess (defined below) are listed in Table 2.

A CO(2–1) line integral map of the brightest CO peak is shown in Figure 6. This map was made at 30″ (full beam) spacing, and the observed positions are indicated by crosses. Some CO emission extends beyond the edges of this map, but the main peak is covered. The full width at half-maximum intensity is $2' \times 1'$. Thus it is evident that there is some structure on scales comparable to the sampling interval (1′–4′) in our 1–0 map, but the brightest clump is clearly recognizable as a single entity at 30″ resolution.

2.2.4. *Minitelescope* CO *Observations*

In order to search for diffuse CO emission and determine the total CO content of G236+39, we have mapped it using the 1.2 m minitelescope at the Center for Astrophysics (CfA) in 1990 December. An area of 1 deg^2 was mapped with full-beam (9′) sampling. The velocity resolution was 0.65 km s^{-1}, which is barely adequate to resolve the CO(1–0) lines. A contour map of these data is shown in Figure 4*b*. Of the 57 map positions, nine had strong lines above the noise level of $\sim$0.1 K. The peak antenna temperature is 0.86 ± 0.09 K for position N. If the 12 m telescope observations resolved the emission, then the ratio of brightness temperatures gives a dilution factor for the 1.2 m telescope beam $\sim$0.3. The dilution factor for the map shown in Figure 6 is only 0.1 averaged over the 1.2 m telescope beam, so

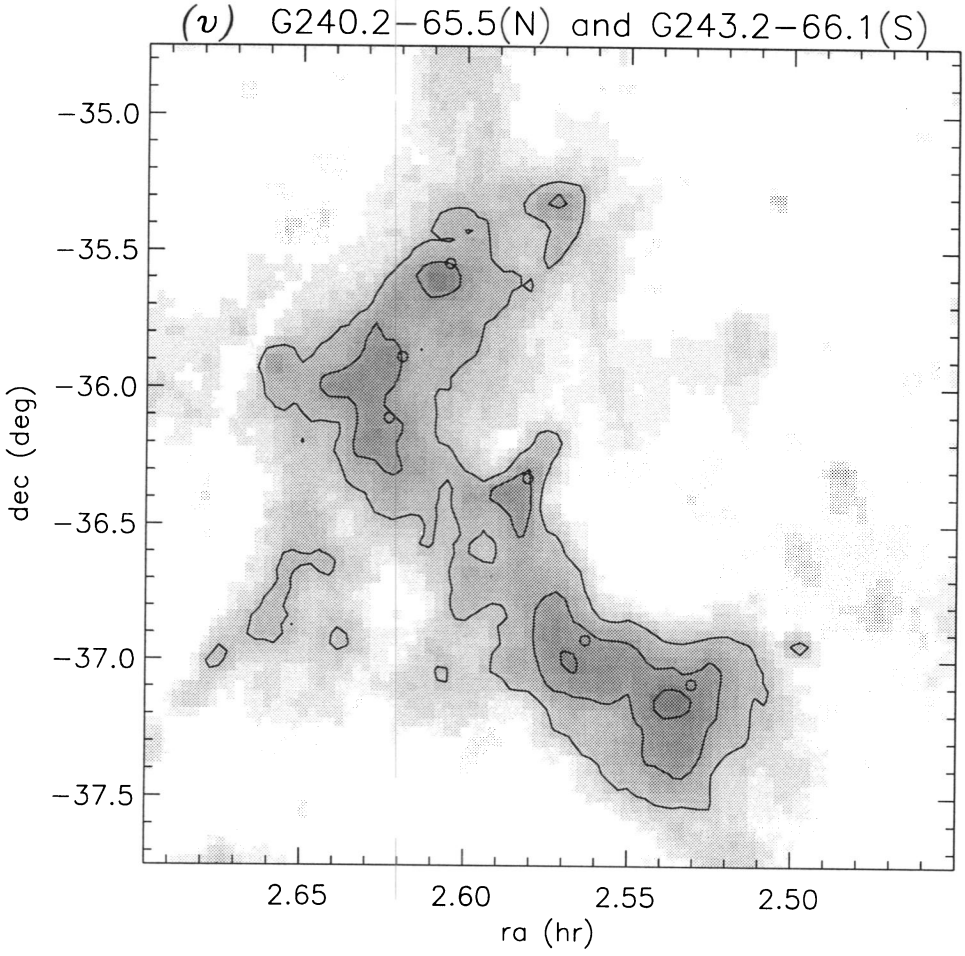

FIG. 1*v*

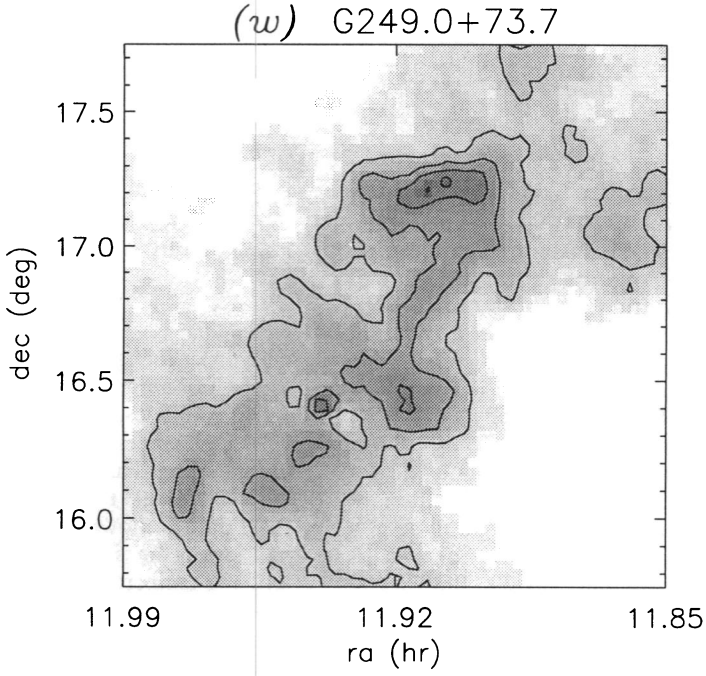

FIG. 1*w*

TABLE 1

SUMMARY OF CO(1–0) SURVEY OF ISOLATED CIRRUS CLOUDS

Cloud	R.A. (1950)	Decl. (1950)	T_R^* (K)	V_0 (km s^{-1})	ΔV (km s^{-1})	Number (NRAO)	Number (CfA)	θ_{CO}[a]
G101.9−62.0.....	00^{h}09^{m}43^s	−00°58′30″	1.4	+2.5	1.9	29		4′
G81.4−77.8.....	00 15 08	−17 51 50	0.5?	+0.4	1.2	3		
G120.1−67.2.....	00 45 23	−04 45 47	<0.4	...	...	2		
G135.4−68.7.....	01 08 21	−06 22 00	1.4	−4.0	0.8	4		
	01 03 39	−06 37 50	2.9	−10.2	0.7	4		
G192.3−67.9.....	02 15 37	−17 59 50	0.4:	−3.8	0.8	2		
G229.0−66.1.....	02 35 28	−30 08 34	<0.2	...	...	1		
G225.6−66.4.....	02 37 27	−31 25 20	4.9	+0.9	0.6	10		6
G243.2−66.1.....	02 33 46	−37 05 10	<0.3	...	...	3		
G240.2−65.5.....	02 37 24	−36 06 40	<0.3	...	...	3		
G228.0−28.6.....	05 26 11	−24 54 00	2.8	−0.8	0.7	16	5	5
G230.1−28.4.....	05 29 42	−26 31 50	2.8	−1.3	0.7	16	1	8
G235.9+38.2.....	09 43 16	+00 57 00	3.9	+8.3	2.0	130	57	12
G235.0+38.7.....	09 43 22	−01 40 00	<0.1	...	...	25	1	
G163.9+59.7.....	10 52 04	+47 20 30	<0.2	...	...	2	25	
G139.6+47.6.....	10 58 12	+65 45 18	0.9	−14.0	0.7	14		4
G141.1+48.0.....	10 49 00	−64 42 58	0.9	−14.2	1.1	19		8
G135.5+51.3.....	11 35 23	+64 17 00	0.5?	−48.0	0.4	5		
G137.3+53.9.....	11 36 20	+61 27 14	<0.3	...	...	2		
G135.3+54.5.....	11 49 21	+61 35 38	0.9	−45.2	1.0	23		4
G149.9+67.4.....	11 49 41	+46 41 30	<0.3	...	...	1		
G249.0+73.7.....	11 54 14	+17 14 30	<0.1	...	...	1		
G126.1+71.6.....	12 46 43	+45 42 20	<0.2	...	...	1		
G107.4+70.9.....	13 18 21	+45 49 12	0.4:	−3.5	0.6	2		
G99.3+68.0.....	13 40 34	+47 10 10	<0.2	...	...	3		
G86.5+59.6.....	14 37 59	+40 16 40	<0.2	...	...	3	49	
G90.0+38.8.....	16 48 07	+59 59 10	4.8	−24.1	1.3	28		20
G94.8+37.6.....	16 48 11	+64 15 32	3.2	−25.0	1.6	35		10
G81.2+39.2.....	16 56 53	+53 00 10	<0.2	...	...	3		
G86.0+38.3.....	16 52 49	+57 22 30	<0.2	...	...	1		
G25.1−67.7.....	23 07 25	−27 34 42	0.5	−7.2	1.2	11		4

[a] Angular size of CO-emitting region.

even toward the peak, the 1.2 m telescope is detecting both the clump and more diffuse emission.

The CO emission is clearly more extended than the ~2′ sized peaks, as can be seen both in the 12 m and 1.2 m telescope maps. The morphology of the 1.2 m telescope map agrees with the undersampled 12 m telescope map, suggesting that little emission was missed. To check this quantitatively, the 12 m telescope map was resampled to simulate the 1.2 m telescope observations. The two maps agree in general, but individual pixels differ; these differences can be attributed to the fact that the NRAO map is undersampled. The total CO fluxes detected by the NRAO and CfA surveys in the area mapped with both telescopes agree to within their uncertainties. There is no evidence for weak, extended CO emission beyond the edge of the NRAO map.

TABLE 2

CO LINES FOR G236+39 PEAKS

Position	Line	T_R^* (K)	ΔV (km s^{-1})	$\int T\,dv$ (K km s^{-1})
N CO peak	CO(1–0)	3.9	2.1	9.2
	CO(2–1)	1.5	2.0	3.0
	^{13}CO(1–0)	0.6	1.7	0.6
	^{13}CO(2–1)	0.4	0.3	0.1
W CO peak	CO(1–0)	3.6	1.7	7.1
	CO(2–1)	1.6	1.4	2.3
	^{13}CO(1–0)	0.4	0.8	0.5
	^{13}CO(2–1)	<0.2	...	...
E CO peak	CO(1–0)	2.0	0.9	1.8
	CO(2–1)	<0.07	...	<0.10
	^{13}CO(1–0)	<0.06	...	<0.06
H_2 peak	CO(1–0)	<0.11	...	<0.16
	^{13}CO(1–0)	<0.04	...	<0.05

3. RESULTS

3.1. *Morphology of Infrared, 21 Centimeter, and CO Emission*

The morphology of the clouds as revealed by CO is clearly different from the infrared morphology, in the sense that the CO emission is more clumped. Inspection of the maps in Figure 1 reveals that there are places in an individual cloud that are equally bright in the infrared, but some have CO emission and some do not. The sensitivity of the CO observations was high enough to detect CO over much larger areas, *if* the CO were distributed as the infrared emission. This phenomenon is shown graphically in Figure 7, where the CO line brightness is plotted against the infrared brightness for all observed locations in Figure 1. There is no simple relation between CO brightness and infrared brightness. The ratio of CO to infrared brightness varies from cloud-to-cloud as well as within individual clouds.

Each of our clouds is associated with enhanced H I 21 cm emission (HRK). The angular resolution of the H I observations (36′) was insufficient to resolve the cores of the clouds. By comparing the infrared surface brightness averaged over an area identical to the H I beam, it was evident that several of the clouds had more infrared emission per H I atom than has been derived for the diffuse interstellar medium (cf. Boulanger & Perault 1988). It is evident from our CO survey that infrared

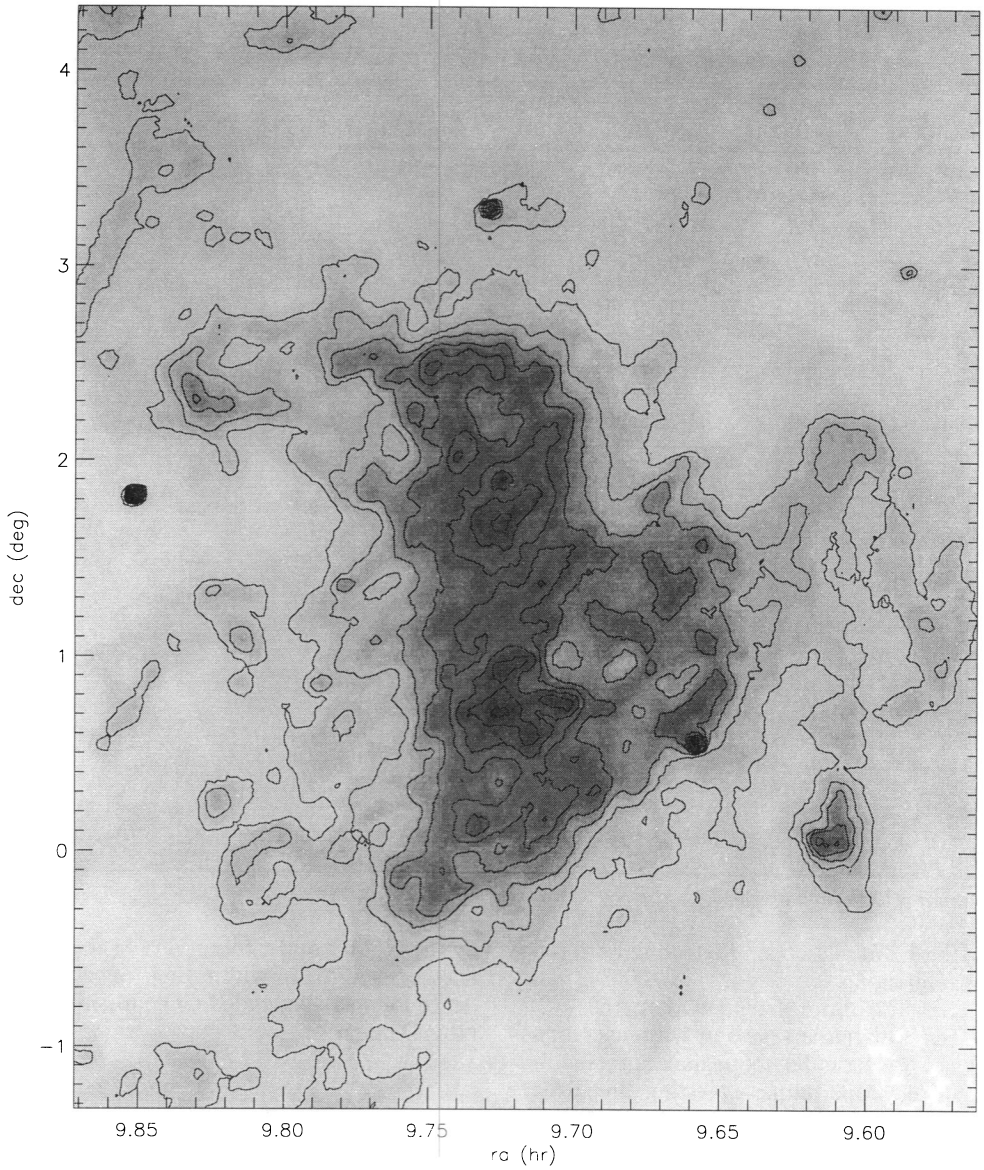

FIG. 2.—A 100 μm surface brightness map of G236+39. This cloud is compsed of three components: a northern cloud with the brightest H I emission ($9^h.72$, $1°.7$), a southern cloud with the brightest infrared and CO emission ($9^h.72$, $0°.8$), and a western "ear" ($9^h.61$, $1°.3$).

excess is present even in clouds with little CO. Let us assume that the infrared emission per nucleon is the same for all clouds to within 30%. Then the column density of H_2 can be inferred from the 100 μm surface brightness, I_{100}, and H I column density, N(H I):

$$N(H_2) = \frac{1}{2}\left[\frac{I_{100}}{\langle I_{100}/N(H)\rangle} - N(\text{H I})\right]. \quad (1)$$

We use $\langle I_{100}/N(H)\rangle = (1 \pm 0.3) \times 10^{20}$ MJy sr^{-1} cm^2 as a representative emissivity per nucleon (HRK; cf. Boulanger & Perault 1988). The CO emission was not mapped fully, so the peak value was diluted by the squared ratio of the angular size of the CO-emitting region (Table 1) to the angular size of the H I observations (HRK). The inferred H_2 column densities are plotted against the diluted CO line integrals in Figure 8. The trend derived by comparing H_2 column densities inferred from γ-ray intensity to the $0°.5$ CO survey of the Galactic plane (Strong et al. 1988) is shown as a solid line, and dashed lines indicate factor of 10 changes in the slope. It is evident that nearly all of our clouds fall to the left of the solid line. The two that lie to the right are part of the Draco nebula, which shows anomalously bright CO emission relative to the inferred H_2 column density. It has been suggested that the dust abundance may be low in the Draco nebula (Reach, Heiles, & Koo 1993), in which case the H_2 column density is underestimated by equation (1). It has also been suggested that the low $N(H_2)/W(CO)$ for the Draco nebula may be related to the interaction of the molecular cloud with incoming high-velocity H I clouds in the vicinity (Herbstmeier et al. 1993). The fact that all of the other clouds fall to the left of the line in Figure 8 suggests that either (1) the ratio of $N(H_2)/W(CO)$ varies from cloud to cloud by an order of magnitude or (2) the H_2 column density is not traced by the CO line integral.

For G236+39, we can see the different morphologies of the

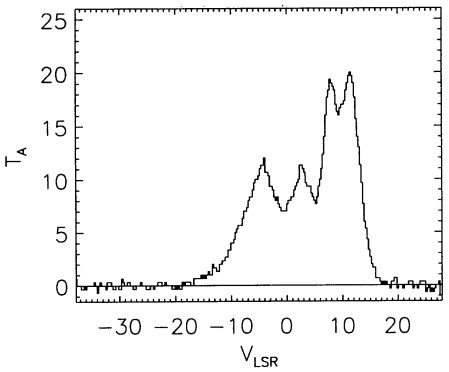

FIG. 3a

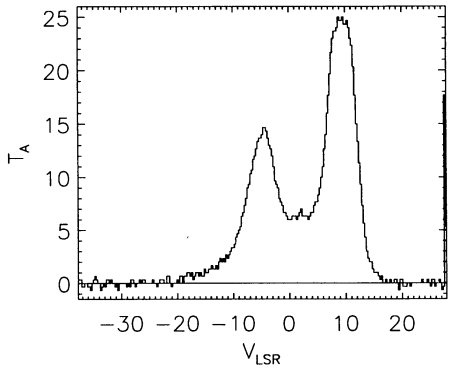

FIG. 3b

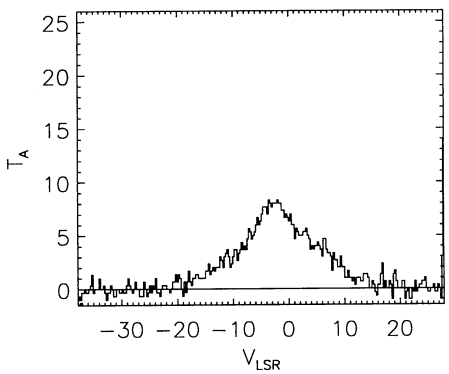

FIG. 3c

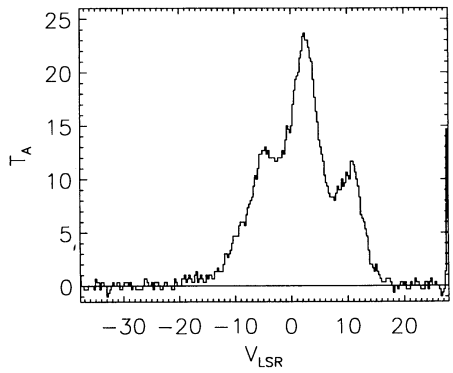

FIG. 3d

FIG. 3.—Sample Arecibo H I spectra for four positions in G236+39: (*a*) CO peak ($9^h43^m12^s$, +00°57′); (*b*) H I peak ($9^h43^m18^s$, +01°57′); (*c*) Off-cloud ($9^h36^m00^s$, +02°57′); and (*d*) Eastern "ear" ($9^h39^m36^s$, +01°33′). The diversity of line profiles allows us to separate the unrelated, diffuse, background gas (which alone forms profile Fig. 3*c*) from the relatively narrow lines of the cloud itself. The northern and southern clouds have similar velocities, while the eastern "ear" is kinematically distinct.

H I, infrared, and CO emission. The H I column density, infrared excess, and CO line integral maps of G236+39 are shown together in Figure 9. These maps were constructed using identical, 3′ grids in equatorial coordinates. H I column densities were calculated from the 21 cm line integrals assuming the line emission is optically thin. The fact that the infrared excess is zero except within the southern cloud core demonstrates the close correspondence between the H I and infrared brightness in the outer parts of the cloud. The fact that the infrared excess is positive in the general region where the CO emission is detected strongly supports our interpretation of infrared excess as an indicator of molecular gas.

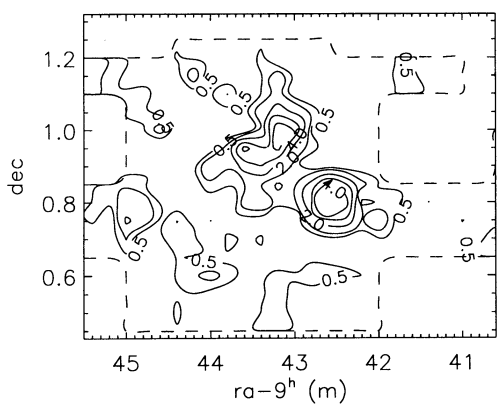

FIG. 4a

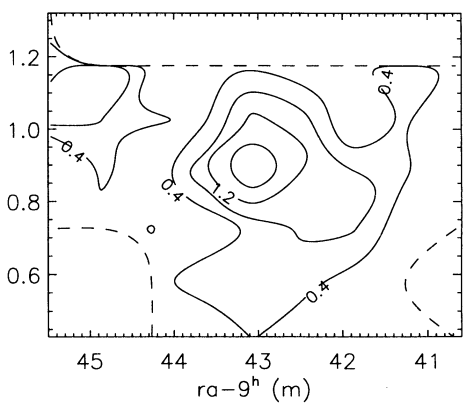

FIG. 4b

FIG. 4.—Maps of the CO(1–0) integrated line emission covering the southern portion of G236+39, where all the CO emission is confined, (*a*) made with the NRAO 12 m telescope and (*b*) the CfA 1.2 m telescope. The dashed contour outlines regions not mapped. While the fully sampled map made with the 1.2 m telescope fails to resolve the emitting regions, it does limit the amount of very extended emission. The map made with the 12 m telescope more closely reveals the morphology of the CO-emitting region, but it suffers from the fact that it is undersampled. The "northern" clump (N), western clump (A), and eastern clump (B) are the three maxima in both of these figures; their spectra are shown in Fig. 5. A higher resolution map of the northern clump, at ($9^h43^m13^s$, 00°56′) is shown in Fig. 6.

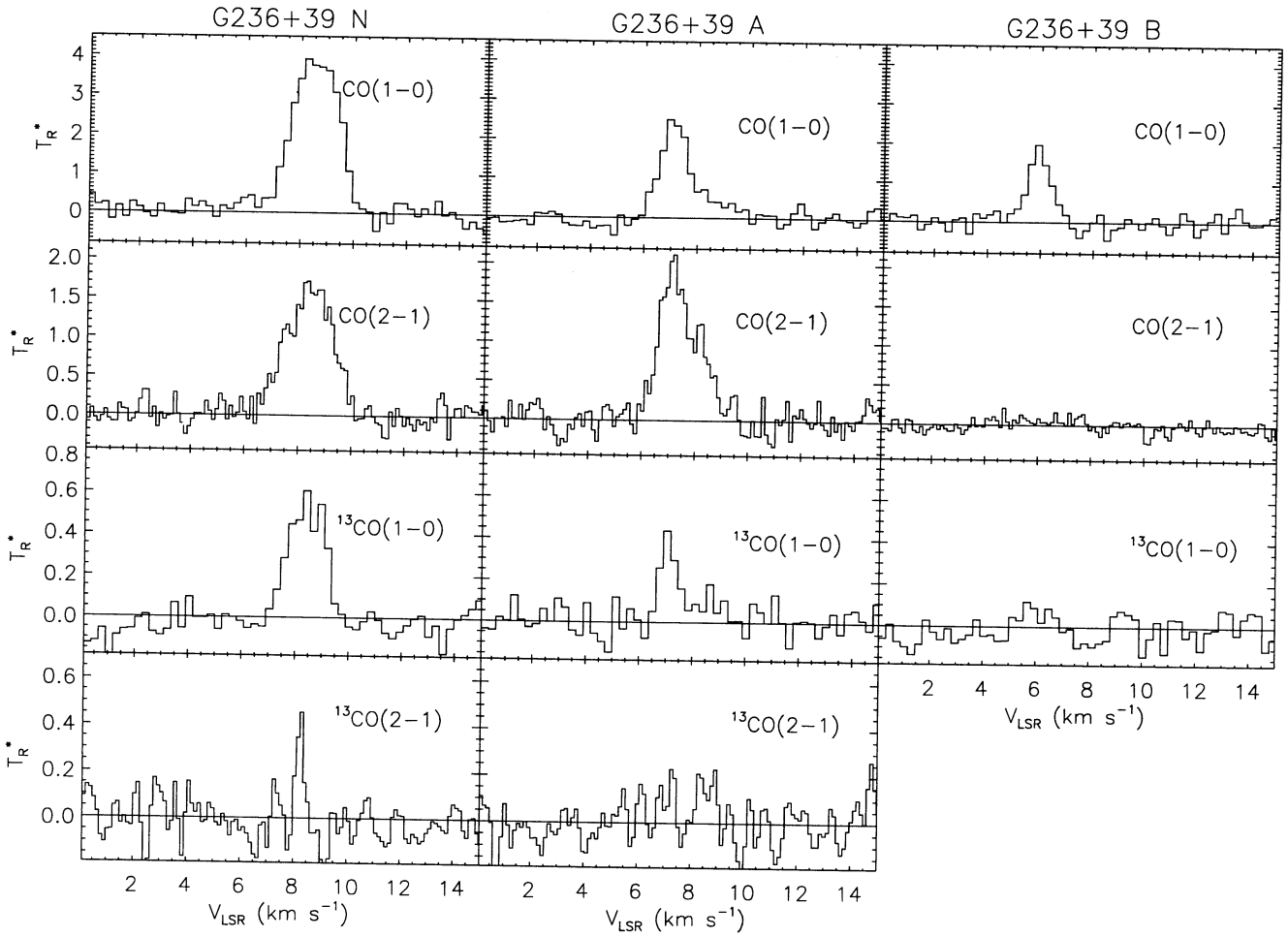

FIG. 5.—Spectra of the CO(1–0) and (2–1) and ^{13}CO(1–0) and (2–1) emission from clumps N, A, and B of cloud G236+39. These three clumps are the primary peaks of the CO(1–0) map. Note the extremely narrow ^{13}CO(2–1) line from clump N.

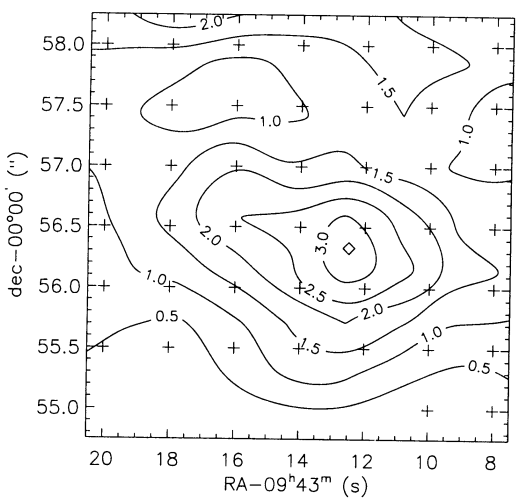

FIG. 6.—Map of the CO(2–1) line integral covering clump N of G236+39. Crosses indicate the observed locations, separated by 30″. The lowest contour is higher than the noise, so low-level emission extends beyond the edge of the map. The full width at half-maximum size of the clump is 2′ × 1′ and is fully contained in this map.

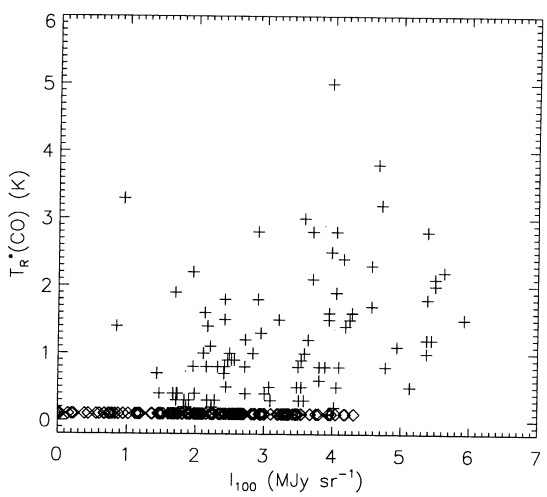

FIG. 7.—The CO(1–0) line brightness is plotted against the infrared (100 μm) surface brightness for all positions indicated in Fig. 1. Diamonds along the bottom indicate nondetections. Note the wide scatter, such that locations with equal infrared brightness may have strong lines in some cases and only weak lines in others. The upper limits for nondetections are lower than 0.2 K, so the survey was not limited by sensitivity.

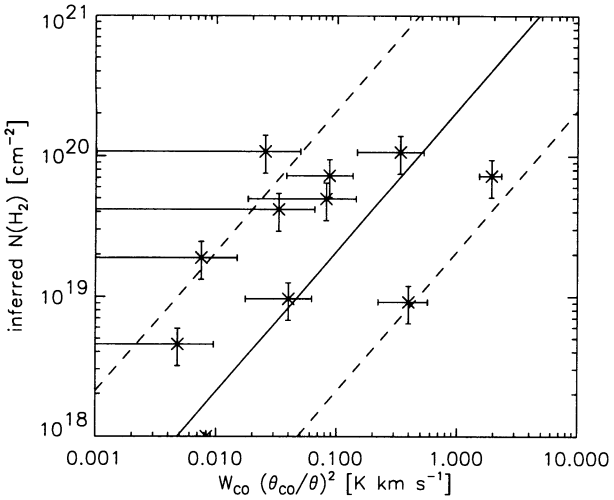

FIG. 8.—The H_2 column density inferred from the excess infrared emission (relative to the H I column density) is plotted against the CO line integral for all clouds in the HRK sample. The infrared and H I column densities refer to $\theta \simeq 36'$ regions, and the CO line is detected over a smaller region of size θ_{CO}, so the CO line integrals are diluted by a factor $(\theta/\theta_{CO})^2$. The solid line indicates the trend inferred for galactic plane clouds using γ-rays, and the dashed lines have factor of 10 larger and smaller slope. The two clouds that fall to the right of the solid line are both in the Draco nebula.

3.2. *Temperature of the* H I *from 21 Centimeter Absorption*

If the 21 cm line emission were smooth on angular scales smaller than twice the Arecibo beam, then the difference between the spectrum toward a continuum source, T_{ON}, and the average of spectra from beams surrounding the source, $\langle T_{OFF} \rangle$, would be a spectrum of the continuum source with 21 cm absorption. Only continuum sources much brighter than the fluctuations in the H I emission on the angular scale of the beam are suitable for this type of experiment. With the Arecibo gain of ~ 3 K Jy^{-1} at high zenith angle, and a typical 21 cm line antenna temperature of 10 K, a suitable continuum source must have a flux $\gg 3\epsilon$ Jy, where ϵ is the fractional amplitude of 21 cm line fluctuations on the angular scale of the beam. Analysis of our 21 cm line channel maps of G236+39 reveals $\epsilon \simeq 0.1$, so that sources with flux $\gg 0.3$ Jy should be suitable. The positions and fluxes (obtained from the 87GB catalog [Gregory & Condon 1991] and 1400 MHz Sky Survey [Condon & Broderick 1985], respectively) of the four bright sources behind G236+39 are listed in Table 3.

For each source, we constructed two fluctuation spectra. The first fluctuation spectrum is the effective absorption spectrum, $\delta T_{ON} = T_{ON} - \langle T_{OFF} \rangle$. The second fluctuation spectrum, δT_{OFF}, is the channel-by-channel rms of the six "OFF" spectra with respect to each other. The maxima of the fluctuation spectra in the velocity range of G236+39 are shown in Table 3. No convincing absorption features were found. Indeed, the strongest features in the "absorption" spectra were often positive. The variation from one reference position to another, as measured by δT_{OFF}, was comparable to or larger than the apparent absorption. Thus true fluctuations in the 21 cm line emission on the angular scale of the beam strongly limit the sensitivity of our experiment. The derived lower limits to the spin temperature are listed in the last column of Table 3. We can conclude that the H I emission is not from very cold gas, and furthermore that the H I profiles are not self-absorbed.

3.3. *Abundance Variations of* CO *Relative to* ^{13}CO

Because they are optically thin, lines of isotopomers of CO are more likely to trace their column densities than the often saturated lines of CO. We obtained ^{13}CO(1–0) observations of the peaks of six clouds, and we observed several positions in G236+39 as well. Some results are shown in Table 4. The limits on the CO/^{13}CO line ratios are very extreme in some cases. If the excitation of the rotational levels were identical for the isotopomers, and the isotopomers occupied the same volume of space, then the line ratio would be determined by the optical depth. In the limit where both CO and ^{13}CO are optically thin, and with the additional assumption that there are no isotope-selective chemical reactions, the line ratio is equal to the abundance ratio of C/^{13}C.

Our observed values of CO/^{13}CO > 90 for two clouds are greater than the solar isotope ratio C/^{13}C = 89, and they are much larger than the interstellar isotope ratio C/^{13}C $\simeq 61 \pm 7$ (Hawkins, Craig, & Meyer 1993; Langer & Penzias 1993). Values of CO/^{13}CO > 60 were also found by Stark (1993) in his radio CO observations of infrared-selected clouds. A high ratio CO/^{13}CO $\gtrsim 80$ was also determined from radio CO observations toward ζ Oph (Lnager et al. 1987). And an extremely high ratio CO/^{13}CO $= 150 \pm 27$ was detected by

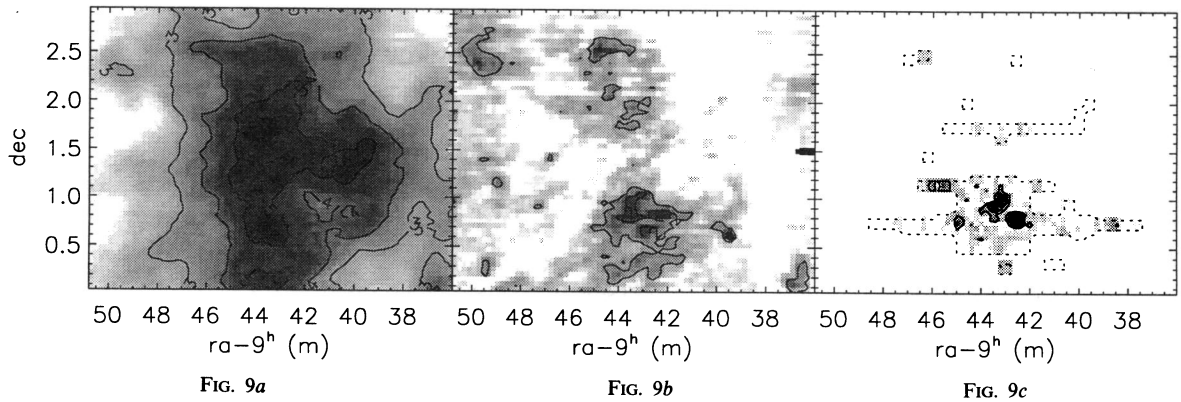

FIG. 9*a* FIG. 9*b* FIG. 9*c*

FIG. 9.—Maps of G236+39 in (*a*) H I column density (contours at 3, 4, 5, 6 × 10^{20} cm^{-2}), (*b*) infrared excess (1, 2, 3 MJy sr^{-1}), and (*c*) CO line integral (1, 2, 5, 8 K km s^{-1}). These maps were made projected onto identical, regular grids with a spacing of 3′ between pixels. The dashed lines in (*c*) outline the region observed for CO. The bright point source in (*b*) at $9^h39^m29^s$, +0°34′ is the galaxy UGC 5180. Note that highest infrared excess occurs in the same general region as the brightest CO line emission, but the infrared excess is more extended.

TABLE 3

21 CENTIMETER ABSORPTION-LINE RESULTS

Source	R.A. (1950)	Decl. (1950)	$F(4850)$ (Jy)	$F(1400)$ (Jy)	$\delta T_{ON}/T$[a]	$\delta T_{OFF}/T$[b]	T_{spin} (K)
PKS 0940+00	$09^h40^m46^s.8$	+00°09′50″	0.53	1.2	0.2	0.7	>30
PKS 0945+003	09 45 50.9	+00 18 34	0.24	1.0	0.8	0.8	>12
3C 230	09 49 24.6	+00 12 46	0.67	3.4	0.1	0.3	>90
PKS 0940+02	09 40 38.0	+02 57 36	0.49	1.1	0.2	0.3	>30

[a] Peak fractional variation between spectrum toward the continuum source and the average spectrum of surrounding positions.

[b] Peak rms variation among reference spectra.

recent *Hubble Space Telescope* ultraviolet observations toward ζ Oph (Sheffer et al. 1992).

Large values of $CO/^{13}CO$ are difficult to explain by gas-phase chemistry. Isotope-selective reactions within clouds would increase the abundance of ^{13}CO relative to CO at low temperatures (van Dishoeck & Black 1988), as is seen to be the case for the resolved CO cores of some clouds (see below). It is possible that for lines of sight with high $CO/^{13}CO$ ratio, the ^{13}CO-emitting regions are smaller than the CO-emitting regions. This is expected for two reasons. First, in the cloud envelope, the CO may be self-shielded but ^{13}CO is not; theoretically, this region is not expected to be large because once CO absorption bands become optically thick, they also begin to absorb the nearby ^{13}CO absorption bands (van Dishoeck & Black 1988). A second explanation could be that the ^{13}CO excitation is substantially different from the CO excitation; this could occur if the cloud envelope has low volume density but is optically thick in the CO line. It is evident from our observations, the observations by Stark (1993), and from comparison between our clouds and dark clouds, that lines of sight with higher CO column densities have a much lower $CO/^{13}CO$ ratio—lower even than the abundance ratio $C/^{13}C$. We conclude that regions with high $CO/^{13}CO$ are cloud peripheries, where the ^{13}CO is either underabundant or not excited.

3.4. *Molecular Excitation*

The CO(1–0), CO(2–1), ^{13}CO(1–0), and ^{13}CO(2–1) spectra for some positions in G236+39 are shown in Figure 5. It is evident that the CO(1–0) line profile is similar to CO(2–1), somewhat wider than ^{13}CO(1–0), and much wider than ^{13}CO(2–1). The 2–1 spectra are spatially weighted averages of maps, with a Gaussian weighting beam equal to that of the 1–0 lines. If the abundance ratio $CO/^{13}CO = 61$, then the observed line ratio suggests that the CO lines have optical depths of $\sim$5–10, and the CO lines may be broadened by saturation. The lines could be optically thin, if the abundance ratio $CO/^{13}CO \simeq 8$. If the emission is spatially resolved, as appears true from the map, then the excitation temperature of the 1–0 transition is 8 ± 1 K.

The excitation of the CO rotational levels is subthermal, as is evident from the low 2–1/1–0 ratio ($\sim$0.4). There is no LTE solution for the low line ratio and column density. Using a large velocity gradient (LVG) model for the excitation and radiative transfer of the CO lines (Goldreich & Kwan 1974; Goldsmith, Young, & Langer 1983), it is possible to match the observed lines *only* in the low-density limit. For kinetic temperatures greater than 10 K, the density limit is $n(H_2) < 800$ cm^{-3}. If we constrain the CO abundance to be less than the cosmic abundance of C, and we further constrain the line-of-sight thickness to be less than twice the observed angular diameter of the emitting region (for a distance of 100 pc), and the kinetic temperature to be less than 100 K, then the density $n(H_2) > 100$ cm^{-3}.

The kinetic temperature of the gas is not well constrained by our observations. The ^{13}CO(2–1) linewidth corresponds to a kinetic temperature of 50 K; this is an upper limit to the actual kinetic temperature because part of the linewidth is nonthermal. The linewidths of the other lines are much greater than that of ^{13}CO(2–1), so these lines may trace different regions. The kinetic temperature of molecular gas in diffuse clouds as determined from ultraviolet absorption lines is 77 ± 17 K (Savage et al. 1977). Using this temperature, the excitation of the CO lines suggests a density $n(H_2) \sim 200$ cm^{-3}.

3.5. *Abundance Variations of* CO *Relative to* H_2

Let us assume for now that the infrared emission traces the total column density of interstellar material, so that the 100 μm

TABLE 4

ISOTOPIC OBSERVATIONS OF CO LINES

Cloud	R.A. (1950)	Decl. (1950)	$T_R^*(^{13}CO)$ (K)	$\Delta V(^{13}CO)$ (km s^{-1})	Line Ratio $(CO/^{13}CO)$
G135.4−68.7	$01^h03^m38^s.9$	−06°37′52″	0.14 ± 0.03	0.3	18
G228.0−28.6	05 26 11.0	−24 54 00	<0.03	...	>90
G230.1−28.4	05 29 42.0	−26 31 50	<0.03	...	>90
G235.9+38.2[a]	09 43 16.0	+00 57 00	0.61 ± 0.07	1.7	6.4
G235.9+38.2[b]	09 44 52.0	+00 45 00	...	>33	
G135.3+54.5	11 47 08.0	+60 27 36	<0.04	...	>13
G90.0+38.8	16 41 17.0	+60 23 08	0.55 ± 0.07	0.5	8.4
G94.8+37.6	16 45 54.0	+64 10 21	<0.03	...	>18

[a] Northern CO peak.

[b] Eastern CO peak.

brightness, $I(100)$, is proportional to the total column density, $N(\mathrm{H})$. The proportionality constant between $I(100)$ and $N(\mathrm{H})$ is determined from the outer parts of the cloud to be 1.1 MJy $\mathrm{sr}^{-1}/10^{20}$ cm^{-2}. The molecular column density is simply determined by the infrared excess: $2N_{\mathrm{IR}}(\mathrm{H}_2) = N(\mathrm{H}) - N(\mathrm{H\ I})$, where the subscript IR indicates a column density inferred from the infrared emission. Note that it is assumed that the H_2 column density is negligible in the outer parts of the cloud. If there is substantial H_2 in the outer parts of the cloud (as is likely based on the ultraviolet studies [Savage et al. 1977] as well as our discussion in § 4.2), then $N_{\mathrm{IR}}(\mathrm{H}_2)$ is an *underestimate* of the true H_2 column density. Now let us compare the inferred H_2 column density to the CO observations.

The spatial correlation between CO and H_2 may be examined by comparing the CO map (Fig. 9*c*) to the infrared excess map (Fig. 9*b*). A slice through G236+39 at declination 00°45′ is shown in Figure 10. The CO peaks are local maxima in the infrared excess map, but the CO emission covers a small fraction of the area with substantial infrared excess. Note that the peak CO brightness is about 20 times the rms noise, while the dynamic range of the inferred H_2 column density is only about a factor of 3. Our observations are sufficiently sensitive to have detected CO over the entire region with inferred H_2 column density larger than 1×10^{20} cm^{-2}. The most extreme case is in the middle of the cloud, where the infrared excess is highest but CO was not even detected.

For comparison with previous work, the infrared map was fitted using a linear combination of the H I column density and CO(1–0) line integral:

$$I_{100} = a[N(\mathrm{H\ I}) + 2XW(\mathrm{CO})] + c\ .$$

A best fit for the CO-observed portion of the cloud is

$$a = (1.50 \pm 0.06) \times 10^{-20}\ \mathrm{MJy\ sr^{-1}\ cm^2}$$

$$X = (0.16 \pm 0.03) \times 10^{20}\ \mathrm{cm^{-2}\ K^{-1}\ km^{-1}\ s}\ .$$

The uncertainties listed above are strictly statistical uncertainties from the fitting procedure. This "best" fit is not a very good approximation of the data. The rms of the residual 100 μm brightness is 0.8 MJy sr^{-1}, and the residuals are spatially correlated—indicating the presence of a component not traced by H I or CO. The "X-factor" for conversion of the CO(1–0) line integral to H_2 is a factor of 16 lower than that found for Galactic plane clouds by comparing the scattered γ-rays to CO maps (Strong et al. 1988) but is similar to the value found for other cirrus clouds (cf. de Vries et al. 1987; Meyerdierks, Brouiller, & Mebold 1990). We conclude that the CO(1–0) line integral *does not* accurately trace the H_2 column density of high latitude clouds.

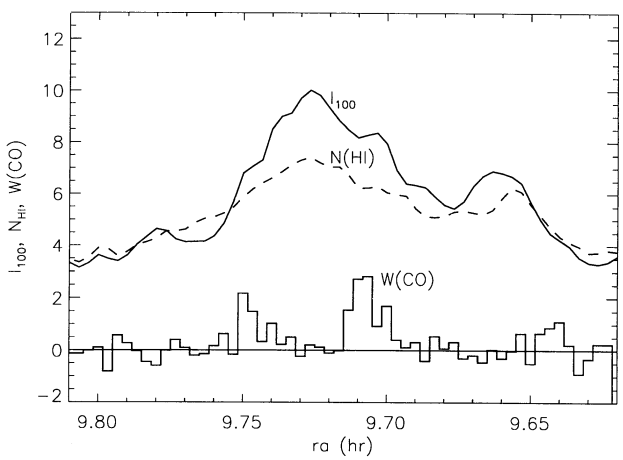

FIG. 10.—Slices through G236+39 at $\delta = 00°45'$ in H I column density (units: 10^{20} cm^{-2}), 100 μm surface brightness (units: MJy sr^{-1}), and CO line integral (units: K km s^{-1}). The infrared emission is more centrally condensed than the H I column density. Molecular gas associated with CO can explain some of the excess infrared emission, but the infrared excess is present in locations where there is no CO, such as between the two CO peaks in this slice.

In order to investigate whether the low $N(\mathrm{H}_2)/W(\mathrm{CO})$ ratio and its strong variations are due to variations in the CO(1–0) line radiative transfer, we observed the ^{13}CO line for several positions in G236+39. Column densities of ^{13}CO were derived for densities and temperatures consistent with the excitation analysis above. These column densities were then compared to the H_2 column density inferred from the infrared excess. It is evident that the abundance of ^{13}CO relative to H_2 (infrared excess) changes by an order of magnitude for any combination of density and temperature consistent with the excitation. (Indeed this same conclusion is obtained in the high-density [LTE] limit.) The most extreme case is in the middle of the cloud. For a kinetic temperature of 80 K and a density of 200 cm^{-3}, the abundance $N(^{13}\mathrm{CO})/N(\mathrm{H}_2) \simeq 4 \times 10^{-6}$ in the CO clumps, while at the cloud center, $N(^{13}\mathrm{CO})/N(\mathrm{H}_2) < 4 \times 10^{-7}$. Therefore the ^{13}CO line is also a poor tracer of H_2 in high-latitude clouds.

4. DISCUSSION

4.1. *Infrared Excess as a Tracer of Molecular Gas*

The infrared map of G236+39 is morphologically identical to the H I map in peripheries of the cloud, and the locations of the CO peaks agree with the strongest local maxima in the infrared map. However, a detailed comparison revealed that the infrared emission is not completely accounted for by a linear combination of the H I and CO maps. Let us define the infrared excess as the difference between the 100 μm map and a scaled H I map. The scaling factor is determined from the outer parts of the cloud, where the H_2 column density is presumed to be small. The infrared excess is confined primarily to the southern cloud core, in a region somewhat larger than the CO emission. While it is likely that the infrared excess is due to dust associated with molecular gas, we consider in the following two subsections alternative explanations.

4.1.1. *Infrared Excess from Enhanced Heating*

To determine whether the excess 100 μm surface brightness is due to enhanced heating of the grains, we compared the infrared excess to the 60/100 μm brightness ratio for the southern cloud core of G236+39. The 60 μm emission from the cloud is quite faint compared to the uncertainty in the background level due to zodiacal emission. We subtracted the brightness of the faintest pixel in a 1° box centered on the southern cloud, and the ratio of the background-subtracted 60 μm and 100 μm maps is shown as a function of the infrared excess in Figure 11. If anything, the color temperature may decrease at the locations of highest infrared excess. The 60 μm emission is probably produced by a combination of the large grains that produce the 100 μm emission as well as a population of small grains (cf. Désert, Boulanger, & Puget 1990), so the 60/100 μm ratio does not directly trace the temperature of the larger grains. However, we can conclude that it is unlikely that the temperature of the larger grains is *enhanced* in the

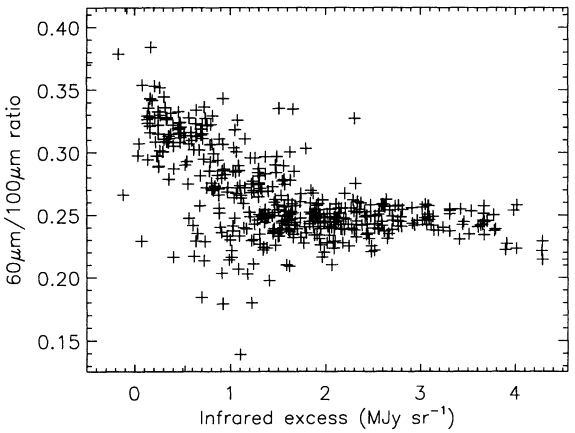

FIG. 11.—The ratio of 60 μm to 100 μm surface brightness is plotted against the infrared excess surface brightness (i.e., the 100 μm surface brightness minus a constant times the H I column density) for each 3′ pixel in a map of the southern component of G236+39. The 60/100 μm ratio does not increase at locations with high infrared excess, as might be expected if the infrared excess is due to enhancement of the grain temperature. Rather, the 60/100 μm ratio may decrease, suggesting either preferential depletion of the smaller grains responsible for the 60 μm emission or a decrease in the grain temperature.

regions of infrared excess, because such a temperature enhancement would almost certainly affect both large and small grains. A decrease in the grain temperature is expected due to shielding of the ultraviolet portion of the radiation field. At the column density corresponding to the onset of lower 60/100 μm ratios, the cloud is opaque to photons shortward of $\sim$3000 Å, which could cause a decrease in the grain temperatures.

There are no bright visible stars near the cloud, nor are there any 12 μm point sources in the cloud. The far-infrared (60–100 μm) point sources within the cloud are apparently unresolved or marginally resolved peaks in the H I and H_2 column density, as well as a few external galaxies. For comparison, a survey of far-infrared sources at high latitudes found 70% of them to be concentrations of interstellar matter, with the remainder mostly external galaxies (Reach et al. 1993).

4.1.2. *Infrared Excess from Enhanced Dust Abundance*

If the dust abundance (relative to H nuclei) or mean cross section were enhanced in the central regions of the cloud, the infrared excess would trace the dust-to-gas ratio. Enhancement of the dust abundance is unlikely because there are no evident dust production sites—for example, stellar envelopes, which would be bright 12 μm sources—within the cloud. Volume densities in the cloud are much too small for dust formation. In dense clouds, molecules freeze onto the surfaces of grains, and perhaps very small grains will stick to the surfaces. The net result would be a *decrease* in the gas phase abundance of molecules that form the grain mantles, and perhaps a decrease in the relative abundance of very small grains. Grain surface chemistry has been found to be important for denser cores of high-latitude molecular clouds, in order to explain the observation that H_2CO abundances decrease toward their centers (Turner 1993). If the molecules and small grains stick to larger grains on each collision, the timescale for them to become depleted onto mantles is of order

$$\tau_{\rm depl} \sim 10^6 \left(\frac{m_g}{m_{\rm H}}\right)^{1/2} \left(\frac{n}{200\ {\rm cm}^{-3}}\right)^{-1} \left(\frac{T}{80\ {\rm K}}\right)^{-1/2} {\rm yr}\ ,$$

where $m_g/m_{\rm H}$ is the mass of the molecule or small grain in units of the H atom mass, and n and T are the gas density and temperature (Draine 1985). For a CO molecule, the depletion time $\sim 6 \times 10^6$ yr, and for a very small grain composed of 60 C atoms, the depletion time $\sim 3 \times 10^7$ yr. These timescales are comparable to interval between successive supernova shocks for a typical location in the interstellar medium. The fact that CO exists in the gas phase at high abundance suggests that accretion is unlikely to be important for the larger molecules, such as polycyclic aromatic hydrocarbons, or for the very small grains. Thus mantle formation is not likely to increase the dust surface area per H atom, not is it likely to cause depletion of the 60 μm emitters, for the diffuse cirrus clouds we are studying.

The ratio of dust mass to gas mass is unlikely to be substantially enhanced except in regions of dust formation. Even in the diffuse interstellar medium, the fraction of the total C abundance locked in grains has been estimated to be $\sim$60% (Tielens & Allamandola 1987). Using the ^{13}CO abundance derived above and $CO/^{13}CO$ abundance ratio of 60, we find that $\sim$30% of the cosmic C abundance is in CO molecules. All of the Si is presumed locked in silicate grains, based on the observed strength of 10 μm absorption lines. Therefore the most abundant and chemically likely building blocks of the grains are used, and enhancements in the dust abundance by factors of several—required to explain the observed variation in infrared brightness relative to gas column density—are highly unlikely.

4.2. *The* H_2/H I *Transition*

Molecular hydrogen is formed on grains, destroyed by photodissociation, and protected by self-shielding in its absorption bands (Hollenbach, Werner, & Salpeter 1971). By calculating the optical depth in each H_2 absorption band and integrating over the radiation field, the total photodissociation rate is found to depend on the H_2 column density as $R \propto N(H_2)^{-1/2}$ in the optically thick limit (Jura 1975). Balancing this rate with the formation rate on grain surfaces,

$$\gamma(T) n({\rm H\ I}) n = R_0\, \beta N(H_2)^{-1/2} n(H_2)\ , \qquad (2)$$

where n(H I), $n(H_2)$, and n are the H I, H_2, and proton (H I + 2 H_2) volume densities, and $N(H_2)$ is the H_2 column density; R_0 is the unshielded photodissociation rate, $\beta N(H_2)^{-1/2}$ is the fractional reduction in the photodissociation rate due to self-shielding, and $\gamma(T)$ is the production coefficient for H_2 on grain surfaces. If the cloud has uniform density (n) and temperature, then we may integrate equation (2) to find

$$N(H_2) = \left(\frac{\gamma}{2R_0\,\beta}\right)^2 n^2 N({\rm H\ I})^2\ .$$

The unshielded photodissociation rate $R_0 \simeq 4.2 \times 10^{-11} \chi\ {\rm s}^{-1}$, using a previous calculation (de Jong, Dalgarno, & Boland 1980) with the ultraviolet radiation field scaled upward to a more recent estimate (Mezger, Mathis, & Panagia 1982, hereafter MMP); the factor χ can be used to scale the radiation field relative to MMP. The H_2 production coefficient $\gamma \simeq 3 \times 10^{-18} T^{1/2}$ cm^3 s^{-1} (van dishoeck & Black 1986). The self-shielding parameter $\beta \simeq 5 \times 10^5$ cm (de Jong et al. 1980).

Combining these values, we obtain

$$N(\mathrm{H_2}) \simeq 4 \times 10^{19} \chi^{-2} \left(\frac{n}{100\ \mathrm{cm^{-3}}}\right)^2 \left(\frac{T}{80\ \mathrm{K}}\right) \times \left[\frac{N(\mathrm{H\ I})}{10^{20}\ \mathrm{cm^{-2}}}\right]^2 \mathrm{cm^{-2}}\ . \quad (3)$$

The equations above apply only if the cloud is old enough to have reached its equilibrium H_2 abundance; lower H_2 abundances are expected for immature clouds. The formation time for H_2 molecules on grain surfaces is of order

$$t_{\mathrm{form}} \simeq \frac{1}{n\gamma} \simeq 2 \times 10^8 \left(\frac{T}{80\ \mathrm{K}}\right)^{-1/2} \left(\frac{n}{50\ \mathrm{cm^{-3}}}\right)^{-1} \mathrm{yr}\ .$$

This timescale is comparable to the mean time between successive supernovae shocks passing through a cloud. Thus low-density clouds rarely have time to develop the equilibrium H_2 abundance predicted by equation (3). Comparisons between the total H_2 and H I column densities along random lines of sight (as traced, e.g., by ultraviolet absorption lines) cannot be expected to yield consistent results unless the H I and H_2 reside in regions of comparable density. Along any line of sight, there is warm, low-density H I ("warm neutral medium," cf. Kulkarni & Heiles 1988) that is not predicted to have any H_2; an advantage of studying individual clouds is that the unrelated H I can be distinguished. Variations in the H_2 chemistry from cloud to cloud are expected due to the frequency of supernovae. Thus some clouds predicted to have large H_2 abundance may in fact be recently shocked.

The width of the transition from atomic to molecular H is

$$L_{\mathrm{tr}} \simeq 0.34 \chi^{1.4} \left(\frac{n}{100\ \mathrm{cm^{-3}}}\right)^{-2.4} \mathrm{pc}$$

(Federman et al. 1979). The sharpness of the atomic-to-molecular hydrogen transition has prevented its direct detection, because it is difficult to achieve high angular resolution in the 21 cm H I line. If the high-latitude clouds are at distances of $\sim 10^2$ pc, based on the thickness of the H I layer of the Galaxy (Lockman et al. 1986), and the density and temperature are typical of cold H I clouds (Kulkarni & Heiles 1988), then the atomic-to-molecular transition occurs on a scale of $\sim 10'$. The transition is resolved by the Arecibo beam as long as the density is less than $\sim 2 \times 10^3$ cm^{-3}, which is true throughout G236+39. The transition would be resolved by the Hat Creek 85 foot (35.9 m) telescope beam (36′) only if the density were less than ~ 5 cm^{-3}, which it almost certainly is not. (In order to be in pressure equilibrium, such low-density gas would have a temperature of $\sim 1 \times 10^3$ K, which is inconsistent with the observed, narrow H I lines.)

Using the Arecibo and *IRAS* maps of G236+39, we are able to resolve the H_2/H I transition. There is an apparent threshold above which the infrared excess is larger than its scatter; we infer that substantial H_2 exists at points in the cloud where the total H column density exceeds $\sim 4 \times 10^{20}$ cm^{-2}. From the scatter plot of the 100 μm brightness versus H I column density, there is a significant positive deviation from a linear correlation, at higher column densities. The proton column density, N(H), can be expressed as a quadratic function of the H I column density, N(H I):

$$I_{100} = aN(\mathrm{H\ I})[1 + N(\mathrm{H\ I})/N_c] + c\ , \quad (4)$$

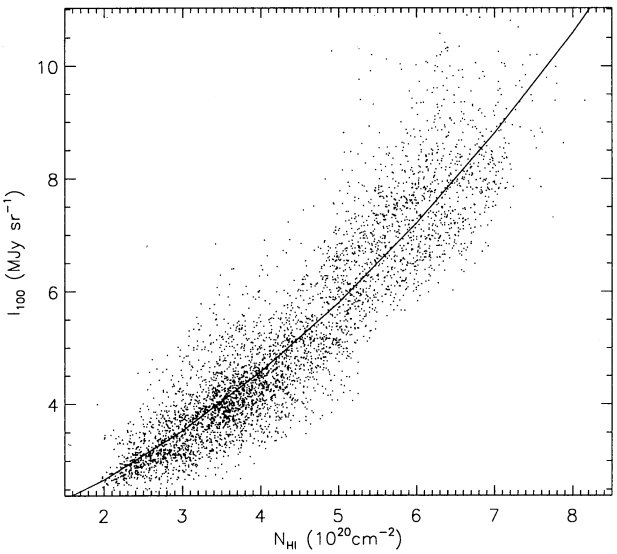

FIG. 12.—The infrared surface brightness for all 21 cm observed positions is plotted against the corresponding H I column density for 4400 independent positions toward the cloud G236+39. Note the nonlinearity of the trend. A linear fit to the lower levels would yield a positive excess at higher levels, which is the infrared excess (presumably due to dust mixed with H_2). A quadratic fit, as predicted for H_2 chemistry, is plotted as a solid curve.

where the second term in the brackets is for H_2. The fit of this equation to our data is shown in Figure 12; we find $N_c = (3.4 \pm 0.5) \times 10^{20}$ cm^{-2}. Using equation (3), with a temperature of 80 K and $\chi = 1$, the volume density required to form H_2 at the observed rate is $n \sim 50$ cm^{-3}. The corresponding thermal pressure is $p/k \simeq 4 \times 10^3$ cm^{-3} K, which is within the range expected for a cloud in pressure equilibrium with the pervasive, warm neutral gas (cf. Kulkarni & Heiles 1988).

The column density and physical conditions we find for the H I–H_2 transition are similar to those found by comparing lines of sight through other diffuse clouds (Federman et al. 1979; Savage et al. 1977). For large molecular clouds ($> 10^3$ $M_\odot$), the H I–H_2 transition occurs in an extended halo, with an extent of ~ 10 pc and density of ~ 50 cm^{-3} (Andersson & Wannier 1993). The column density through these halos is $\gtrsim 10^{21}$ cm^{-2}, larger than the column density where substantial H_2 forms in diffuse clouds (cf. Federman et al. 1979). The halos may owe their existence to the fact that H_2 formation is inefficient on icy grains, such as found at high extinction (Andersson & Wannier 1993).

The model for H_2 formation and the model for CO excitation given different results for the volume density of G236+39. The CO excitation analysis refers to a much smaller portion of the cloud, so there could be a mild, large-scale density gradient ($n \propto r^{-0.6}$) or a sudden density enhancement in the core. For a cloud confined by external pressure, p_{ext}, the pressure at cloud center, p_0, is enhanced due to self-gravity:

$$\frac{p_0}{p_{\mathrm{ext}}} = 1 + \left(\frac{p_{\mathrm{ext}}/k}{10^4\ \mathrm{cm^{-3}\ K}}\right)^{-1} \left[\frac{N(\mathrm{H})}{3.1 \times 10^{21}\ \mathrm{cm^{-2}}}\right]^2 ,$$

where N(H) is the total (H I + 2H_2, front-to-back) column density of the cloud (cf. van Dishoeck & Black 1986). For G236+39, the central pressure is $\lesssim 30\%$ larger than the external pressure. The total pressure is a sum of thermal (gas) pressure and the nonthermal pressure due to turbulent motions and Alfvén waves (cf. Myers & Goodman 1988). In the CO

cores, the nonthermal pressure inferred from the ratio of ^{13}CO linewidth to the H I linewidth is ~ 4 times smaller in the core than the outer parts of the cloud. Thus the thermal pressure must increase by a factor ~ 5 in the cores in order for the cloud and cores to be in hydrostatic equilibrium. The ratio of the volume density inferred for CO excitation (in the cores) and H_2 formation (in the cloud) is a factor of 8. Thus if the core temperature is ~ 50 K, which is consistent with the CO excitation, the cloud could be in hydrostatic equilibrium.

4.4. *Completely Atomic Clouds*

Some of the clouds in our sample are predominantly atomic, and the lack of H_2 can be used to set an upper limit to the density using equation (3). For a purely atomic cloud, the infrared brightness will be linearly proportional to the H I column density. In Figure 13, we compare the 100 μm surface brightness to the H I column density for G249+73.7, which we mapped (132 spectra) at Arecibo. The 21 cm line was integrated only over the low-velocity component of the spectral line, which is associated with the cloud. Another small cloud, G9+51, was partially mapped at Arecibo with similar results: the infrared surface brightness is linearly proportional to the cloud column density between 0.5 and 2.0×10^{20} cm^{-2} (Herter, Shupe, & Chernoff 1990). A quadratic fit of equation (4) for G249.0+73.7 yields a negative coefficient for the second-order term, so we use the uncertainty in the coefficient to derive an upper limit to the H_2 column density at any position. Using equation (3), the upper limit (95% confidence) on the density for G249+73.7 is

$$n < 70\chi\left(\frac{T}{80\ \mathrm{K}}\right)^{-1/2}\ \mathrm{cm}^{-3}\ .$$

This upper limit is not strict; it allows a density comparable to that of G236+39. Thus the principal difference between G249.0+73.7 and G236+39 may be simply size; a smaller cloud does not have as much H_2 because the column density is insufficient for substantial self-shielding.

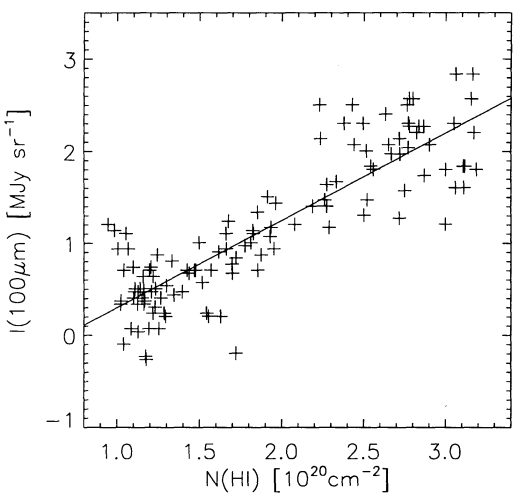

FIG. 13.—The infrared surface brightness is plotted against the corresponding H I column density for 132 independent lines of sight toward the cloud G249+73.7. The best linear fit is shown as a solid line. The best quadratic fit is indistinguishable, so only an upper limit to the H_2 column density can be established.

4.4. *Regions of Enhanced* CO *Abundance*

In G236+39, we are able to locate another transition: the location where the CO abundance increases by more than an order of magnitude. Theoretical calculations of the CO photodissociation and chemistry resulted in abundances CO/$H_2 \sim 10^{-4}$ for clouds with $A_V > 1$ and CO/$H_2 \sim 10^{-6}$ for $A_V < 0.3$ (van Dishoeck & Black 1988). At positions with detected CO, our inferred CO abundance is similar to that of an opaque cloud, while at positions of nondetections, the abundances are even less than for a diffuse cloud. The column density above which CO is detected corresponds to $A_V \simeq 0.5$, in good agreement with models of CO formation in translucent clouds (van Dishoeck & Black 1988). The strong *variations* in the CO abundance, however, cannot be easily explained by photodissociation. The variations may be due to time-dependent chemistry differences. The dynamical timescale $2R/\Delta V \sim 6 \times 10^5$ yr for the clouds is comparable to the chemical timescale for forming CO, so it is likely that the CO abundance never reaches its equilibrium value. The CO-rich regions may be regions in which the chemistry has achieved somewhat greater maturity than in neighboring regions.

5. CONCLUSIONS

A survey of isolated interstellar cirrus clouds for CO emission revealed CO emitting regions that are typically 2′–10′ in size, while the infrared and 21 cm emission extend throughout the clouds. The infrared emission per H atom is enhanced in clouds with detected CO, suggesting that the excess emission is from dust associated with molecular gas. Assuming the infrared excess is from dust associated with H_2, and the emission per H-nucleon is the same in atomic and molecular gas, we infer an average H_2 column density for each cloud that is *not* well correlated with the integrated CO emission.

High angular resolution Arecibo H I and NRAO CO maps of one cloud, G236+39, allowed us to spatially resolve the variations of infrared brightness, H I column density, and CO line integral. The infrared excess is unlikely to be produced by enhanced heating in the cloud, since no heating sources are evident; furthermore, the 60/100 μm color temperature decreases in the regions of infrared excess. Thus we interpret the infrared excess as an indicator of the presence of H_2. The infrared excess and CO line integral are highest in the same general portion of the cloud, but they are poorly correlated in detail. The same conclusion is reached for the ^{13}CO column density. The regions of infrared excess are larger than the regions with detectable radio CO lines, despite the fact that our CO observations had enough sensitivity to detect lines throughout most of the infrared excess region. The abundance of ^{13}CO relative to H_2 must increase by at least an order of magnitude in the regions of detectable CO lines. Thus the CO lines are a poor tracer of H_2 column density in diffuse clouds.

By comparing the H I and infrared maps of G236+39, the transition from atomic to molecular gas was resolved. The variation of total column density with atomic column density can be explained by a model of H_2 formation on grain surfaces balanced by self-shielded photodissociation. The critical column density for H_2 formation inferred by fitting the model to the observations is consistent with plausible physical conditions in the cloud ($n \sim 50$ cm^{-3} for $T = 80$ K). The results suggest that $\sim 40\%$ of H nuclei are in H_2 molecules. Thus even the cloud periphery contains molecular hydrogen. This is in agreement with previous studies of the H_2/H I transition based

on ultraviolet observations of absorption lines due to H I and H_2 (Savage et al. 1977; Federman et al. 1979). Thus even for cirrus clouds, comparisons of the infrared brightness to the H I 21 cm line integral must take diffuse H_2 into account. Given an estimate for the density and temperature of a cloud, equation (3) can be used to calculate the H_2 column density as a function of the H I column density. The ratio of H_2 mass to H I mass is

$$\frac{M(H_2)}{M(H\,I)} = 0.23 \times 10^{-20}\left(\frac{n}{50\ \mathrm{cm}^{-3}}\right)^2\left(\frac{T}{80\ \mathrm{K}}\right)\frac{\langle N(H\,I)^2\rangle}{\langle N(H\,I)\rangle},$$

where angle brackets indicate averaging over the cloud. If the H I observations do not resolve the H_2 region, this is a *lower* limit. Using the low-resolution H I survey of HRK, and assuming a density for all clouds comparable to that of G236+39, the H_2 mass ranges from >7% to >50% of the cloud mass. Using the Arecibo map of G236+39, and an assumed distance of 100 pc, the mass of H I is 90 $M_\odot$, and the mass of H_2 is 70 $M_\odot$. Thus the mass of cirrus clouds can be substantially greater than the mass of atomic gas.

This work was supported in part by a NASA (Astrophysics Data Program) grant to C. H. and in part by NSF Award 88-18544 and 91-23362 to C. H. W. T. R. was supported by a National Research Council Resident Associateship while at NASA/GSFC. P. Jewell is thanked for help with the operation and calibration of the NRAO 12 m telescope, and Loris Magnani is thanked for help with the observations at the NAIC 305 m telescope. We thank S. Digel and T. Dame for help with the CfA 1.2 m telescope observations. C. S. Tamanaha is gratefully thanked for going to Arecibo to perform the 21 cm line observations, and P. R. McCullough is thanked for lending a hand during the NRAO 12 m telescope observations.

REFERENCES

Andersson, B-G, & Wannier, P. G. 1993, ApJ, 402, 585
Blitz, L., Bazzell, D., & Désert, F.-X. 1990, ApJ, 352, L13
Boulanger, F., & Perault, M. 1988, ApJ, 330, 964
Condon, J. J., & Broderick, J. J. 1985, AJ, 90, 2540
de Jong, T., Dalgarno, A., & Boland, W. 1980, A&A, 91, 68
Désert, F.-X., Bazell, D., & Boulanger, F. 1988, ApJ, 334, 815
Désert, F.-X., Boulanger, F., & Puget, J.-L. 1990, A&A, 237, 1
de Vries, H. W., Heithausen, A., & Thaddeus, P. 1987, ApJ, 319, 723
Dickey, J. M. 1977, Ph.D. thesis, Cornell Univ.
Draine, B. T. 1985, in Protostars and Planets II, ed. D. C. Black & M. S. Matthews (Tucson: Univ. of Ariz. Press), 621
Federman, S. R., Glassgold, A. E., & Kwan, J. 1979, ApJ, 227, 466
Goldreich, P., & Kwan, J. 1974, ApJ, 189, 441
Goldsmith, P. F., Young, J. S., & Langer, W. D. 1983, ApJS, 51, 203
Gregory, P. C., & Condon, J. J. 1991, ApJS, 75, 1011
Hawkins, I., Craig, N., & Meyer, D. M. 1993, ApJ, 407, 185
Heiles, C., & Habing, H. J. 1974, A&AS, 14, 1
Heiles, C., Reach, W. T., & Koo, B.-C. 1988, ApJ, 332, 313 (HRK)
Heithausen, A., Stacey, J. G., de Vries, H. W., Mebold, U., & Thaddeus, P. 1993, A&A, 268, 265
Herbstmeier, U., Heithausen, A., & Mebold, U. 1993, A&A, 272, 514
Herter, T., Shupe, D. L., & Chernoff, D. F. 1990, ApJ, 352, 149
Hollenbach, D. J., Werner, M. W., & Salpeter, E. E. 1971, ApJ, 163, 165
Jura, M. 1975, ApJ, 197, 575
Keto, E. R., & Myers, P. C. 1986, ApJ, 304, 466
Kulkarni, S. R., & Heiles, C. 1988, in Galactic and Extragalactic Radio Astronomy, ed. G. L. Verschuur & K. I. Kellerman (New York: Springer-Verlag), 95
Langer, W. D., Glassgold, A. E., & Wilson, R. W. 1987, ApJ, 322, 450
Langer, W. D., & Penzias, A. A. 1993, ApJ, 408, 539
Lockman, F. J., Hobbs, L. M., & Shull, J. M. 1986, ApJ, 301, 380
Martin, P. G., Rogers, C., Reach, W. T., Dewdney, P. E., & Heiles, C. 1993, in The First Symposium on the Infrared Cirrus and Diffuse Interstellar Clouds, ed. W. Latter & R. Cutri (ASP Conf. Ser.), in press
Meyerdierks, H., Brouillet, N., & Mebold, U. 1990, A&A, 230, 172
Mezger, P. G., Mathis, J. S., & Panagia, N. 1982, A&A, 105, 372 (MMP)
Meyers, P. C., & Goodman, A. A. 1988, ApJ, 329, 392
Neugebauer, G., et al. 1984, ApJ, 278, L1
Reach, W. T., Heiles, C., & Koo, B.-C. 1993, ApJ, 412, 127
Rohlfs, R., Herbstmeier, U., Mebold, U., & Winnberg, A. 1989, A&A, 211, 402
Savage, B. D., Bohlin, R. C., Drake, J. F., & Budich, W. 1977, ApJ, 216, 291
Sheffer, Y., Federman, S. R., Lambert, D. L., & Cardelli, J. A. 1992, ApJ, 397, 482
Spitzer, L., & Jenkins, E. B. 1975, ARA&A, 13, 133
Stark, A. A., Gammie, C. F., Wilson, R. W., Bally, J., Linke, R. A., Heiles, C., & Hurwitz, M. 1992, ApJS, 79, 77
Stark, R. 1993, Ph.D. thesis, Sterrewacht Leiden
Strong, A. W., Bloeman, J. B. G. M., Dame, T. M., Grenier, I. A., Hermsen, W., Lebrun, F., Pollock, A. M. T., & Thaddeus, P. 1988, A&A, 207, 1
Tielens, A. G. G. M., & Allamandola, L. J. 1987, in Interstellar Processes, ed. D. J. Hollenbach & H. A. Thronson, Jr. (Dordrecht: Reidel), 397
Turner, B. E. 1993, ApJ, 410, 140
van Dishoeck, E. F., & Black, J. H. 1986, ApJS, 62, 109
———. 1988, ApJ, 334, 771
Wheelock, S., et al. 1991, *IRAS* Sky Survey Atlas (IPAC/JPL: Pasadena) (ISSA)